



1

2 **Impacts of air pollutants from fire and non-fire emissions on the regional**

3 **air quality in Southeast Asia**

4 Hsiang-He Lee^{1@}, Oussama Iraqui², Yefu Gu³, Hung-Lam Steve Yim³, Apisada

5 Chulakadabba⁴ Adam Y. M. Tonks⁵, Zhengyu Yang⁶, and Chien Wang^{1,7}

6

7 ¹Center for Environmental Sensing and Modeling, Singapore-MIT Alliance for Research
8 and Technology, Singapore

9 ²Energy and Environmental Engineering Department, National Institute of Applied Science
10 of Lyon (INSA Lyon), France

11 ³Department of Geography and Resource Management, The Chinese University of Hong
12 Kong, Hong Kong

13 ⁴Department of Civil & Environmental Engineering, Massachusetts Institute of Technology,
14 Cambridge, MA, U.S.A.

15 ⁵Division of Science, Yale-NUS College, Singapore

16 ⁶Department of Mathematics, National University of Singapore, Singapore

17 ⁷Center for Global Change Science, Massachusetts Institute of Technology, Cambridge,
18 MA, U.S.A.

19

20

21

22

23

24

25

26

27 [@]Corresponding author address: Dr. Hsiang-He Lee, 1 CREATE Way, #09-03 CREATE

28 Tower, Singapore, 138602

29 E-mail: hsiang-he@smart.mit.edu

30



31 Abstract

32 Severe haze events in Southeast Asia caused by particulate pollution have become
33 more intense and frequent in recent years, degrading air quality, threatening human
34 health, and interrupting economic and societal activities. Widespread biomass burning
35 activities are a major source of severe haze events in Southeast Asia. On the other hand,
36 particulate pollutants from human activities other than biomass burning also play an
37 important role in degrading air quality in Southeast Asia. In this study, numerical
38 simulations have been conducted using the Weather Research and Forecasting (WRF) model
39 coupled with a chemistry component (WRF-Chem) to quantitatively examine the
40 contributions of aerosols emitted from fire (i.e., biomass burning) versus non-fire (including
41 fossil fuel combustion, road and industrial dust, land use, and land change, etc.) sources to
42 the degradation of air quality and visibility over Southeast Asia. These simulations cover a
43 time period from 2002 to 2008 and were respectively driven by emissions from: (a) fossil
44 fuel burning only, (b) biomass burning only, and (c) both fossil fuel and biomass burning.
45 Across ASEAN 50 cities, these model results reveal that 39% of observed low visibility
46 days can be explained by either fossil fuel burning or biomass burning emissions alone, a
47 further 20% by fossil fuel burning alone, a further 8% by biomass burning alone, and a
48 further 5% by a combination of fossil fuel burning and biomass burning. The remaining
49 28% of observed low visibility days remain unexplained, likely due to emissions sources
50 that have not been accounted for. Further analysis of 24-hr $PM_{2.5}$ Air Quality Index (AQI)
51 indicates that comparing to the simulated result of the case with stand-alone non-fire
52 emissions, the case with coexisting fire and non-fire $PM_{2.5}$ can substantially increase the
53 chance of AQI being in the moderate or unhealthy pollution level from 23% to 34%. The
54 premature mortality among major Southeast Asian cities due to degradation of air quality by



55 particulate pollutants is estimated to increase from ~4110 per year in 2002 to ~6540 per year
56 in 2008. In addition, we demonstrate the importance of certain missing non-fire
57 anthropogenic aerosol sources including anthropogenic fugitive and industrial dusts in
58 causing urban air quality degradation. An exploratory experiment of using machine learning
59 algorithms to forecasting the occurrence of haze events in Singapore is also demonstrated in
60 this study. All these results suggest that besides minimizing biomass burning activities, an
61 effective air pollution mitigation policy for Southeast Asia needs to consider controlling
62 emissions from non-fire anthropogenic sources.

63 **1 Introduction**

64 Severe haze in Southeast Asia has attracted the attention of governments and the
65 general public in the recent years due to its impact on local economy, air quality and public
66 health (Miettinen et al., 2011; Kunii et al., 2002; Frankenberg et al., 2005; Crippa et al.,
67 2016). Widespread biomass burning activities are one of the major sources of haze events in
68 Southeast Asia. Our previous study demonstrated that biomass burning aerosols contributed
69 to up to 40-60% of haze events in the major cities of Southeast Asia during 2003-2014 (Lee
70 et al., 2017). On the other hand, biomass burning in Southeast Asia could impact climate
71 through emissions of both carbon dioxide (CO₂) (van der Werf et al., 2009) and particulate
72 matter – the latter has a substantial impact specifically on regional climate features including
73 the spatiotemporal distribution of precipitation and energy budgets (Wang, 2004, 2007).

74 Regarding the impact of biomass burning aerosols on public health, a recent study based
75 on the health model in the United States (U.S.) has estimated the number of deaths resulting
76 from black carbon (BC) to be more than 13,500 in 2010 (Li et al., 2016). Considering that
77 both the ambient concentration of particulate matter and overall population in Southeast



78 Asia are higher than those of the U.S., a worse scenario in the region could thus be
79 foreseeable. In fact, a few studies quantifying the consequences of aerosols on human
80 health in Southeast Asia have already suggested taking necessary measures to reduce
81 biomass burning and deforestation in order to prevent related public health issues (Marlier et
82 al., 2013). However, as important as biomass burning pollution may be, it is not the only
83 source of particulate pollution in Southeast Asia. Indeed, aerosols emitted from fossil fuel
84 burning alongside other non-biomass burning human activities, as indicated in our previous
85 study (Lee et al., 2017), also contribute significantly to air quality degradation.

86 Particulate pollutants from human activities other than biomass burning in Southeast
87 Asia include species both locally produced and brought in from neighboring regions by
88 long-range transport. Fossil fuel emissions in Southeast Asia have increased significantly in
89 recent years, especially in areas where energy demands are growing rapidly in response to
90 economic expansion and demographic trends (IEA, 2015). Therefore, advancing our
91 understanding of the respective contributions of aerosols from fire (i.e., biomass burning)
92 versus non-fire (including fossil fuel combustion, road and industrial dust, land use, and land
93 change, etc.) activities to air quality and visibility degradation has become an urgent task for
94 developing effective air pollution mitigation policies in Southeast Asia.

95 In this study, we aim to examine and quantify the impacts of fire and non-fire aerosols
96 on air quality and visibility degradation over Southeast Asia. Three numerical simulations
97 have been conducted using the Weather Research and Forecasting (WRF) model coupled
98 with a chemistry component (WRF-Chem), driven respectively by aerosol emissions from:
99 (a) fossil fuel burning only, (b) biomass burning only, and (c) both fossil fuel and biomass
100 burning. By comparing the results of these experiments, we examine the corresponding
101 impacts of fossil fuel and biomass burning emissions, both separately and combined, on the



102 air quality and visibility of the region. We firstly describe methodologies adopted in the
103 study, followed by the results and findings from our assessment of the relative contributions
104 of fire and non-fire aerosols in degrading air quality and visibility over Southeast Asia. We
105 then discuss the uncertainty of current emission inventories alongside the results from an
106 exploratory experiment of using machine learning algorithms to forecasting the occurrence
107 of haze events in several major cities in Southeast Asia. The last section summarizes and
108 concludes our work.

109 **2 Methodology**

110 **2.1 Observational data**

111 **2.1.1 Surface visibility**

112 The observational data of surface visibility from the Global Surface Summary of the
113 Day (GSOD) (Smith et al., 2011) are used in our study to identify the days with low
114 visibility due to particulate pollution, i.e., haze events. The GSOD is derived from the
115 Integrated Surface Hourly (ISH) dataset and archived at the U.S. National Climatic Data
116 Center (NCDC). The daily visibility data are available from 1973 onward.

117 **2.1.2 Particulate matter (PM₁₀)**

118 The surface concentrations of particulate matter with sizes smaller than 10 μm (PM₁₀;
119 measured in $\mu\text{g m}^{-3}$) in Malaysia are derived from the Air Quality Index (AQI; named Air
120 Pollutant Index or API in Malaysia) records obtained from the website of Ministry of
121 Natural Resources and Environment, Department of Environment, Malaysia
122 (http://apims.doe.gov.my/public_v2/home.html). When PM₁₀ is reported as the primary
123 pollutant with a maximum pollutant index, the 24-hr PM₁₀ concentrations are calculated
124 from AQI based on the equations in Table S1(Malaysia, 2000). Data from 51 AQI



125 observation stations are available in Malaysia from October 2005 onward. AQI number is
126 reported twice daily (11 AM and 5 PM local time), and the data reported at 11 AM are used
127 in this study.

128 **2.1.3 Carbon monoxide (CO) and ozone (O₃)**

129 The surface mole fractions of CO and O₃ are observed from the World Meteorological
130 Organization (WMO) Global Atmosphere Watch (GAW) station in Bukit Kototabang,
131 which is located on the island of Sumatra, Indonesia. Hourly data are archived at the World
132 Data Center for Greenhouse Gases (WDCGG) under the GAW program
133 (<http://ds.data.jma.go.jp/gmd/wdcgg/>).

134 **2.1.4 Crustal matter and residual matter**

135 The Surface PARTiculate mAtter Network (SPARTAN) is a network of ground-based
136 measurements of fine particle concentrations (<http://spartan-network.weebly.com/>)
137 (Snider et al., 2016; Snider et al., 2015). Available data in the SPARTAN network include
138 hourly PM_{2.5} concentrations and certain compositional features (Table S2). Crustal matter
139 and residual matter from filtered PM_{2.5} samples are used in this study to fill the gap in
140 modeled PM_{2.5} created by the missing anthropogenic dust in emission inventory (Philip et
141 al., 2017). The four operational SPARTAN sites in Southeast Asia are Bandung (Indonesia),
142 Hanoi (Vietnam), Manila (Philippine), and Singapore (Singapore).

143 **2.2 The model**

144 WRF-Chem version 3.6.1 is used in this study to simulate trace gases and particulates
145 interactively with the meteorological fields using several treatments for photochemistry and
146 aerosols (Grell et al., 2005). We selected the Regional Acid Deposition Model, version 2
147 (RADM2) photochemical mechanism (Stockwell et al., 1997) coupled with the Modal



148 Aerosol Dynamics Model for Europe (MADE), which includes the Secondary Organic
149 Aerosol Model (SORGAM) (Ackermann et al., 1998; Schell et al., 2001), to simulate
150 anthropogenic aerosols evolution in Southeast Asia. MADE/SORGAM uses a modal
151 approach (including Aiken, accumulation, and coarse modes) to represent the aerosol size
152 distribution, and predicts mass and number for each aerosol mode. The numerical
153 simulations are employed within a model domain with a horizontal resolution of 36 km,
154 including 432×148 horizontal grid points (Fig. 1), and 31 vertically staggered layers based
155 on a terrain-following pressure coordinate system. The domain covers an area from the
156 Indian Ocean to Western Pacific Ocean in order to capture the Madden-Julian Oscillation
157 (MJO) pattern. The time step is 180 seconds for advection and physics calculation. The
158 physics schemes included in the simulations are listed in Table 1. The initial and boundary
159 meteorological conditions are taken from the U.S. National Center for Environment
160 Prediction FiNaL (NCEP-FNL) reanalysis data (National Centers for Environmental
161 Prediction, 2000), which has a spatial resolution of 1 degree and a temporal resolution of 6
162 hours. Sea surface temperatures are updated every 6 hours in NCEP-FNL. All simulations
163 used a four-dimensional data assimilation (FDDA) method to nudge NCEP-FNL
164 temperature, water vapor, and zonal as well as meridional wind speeds above the planetary
165 boundary layer (PBL).

166 **2.3 Emission inventories**

167 The Regional Emission inventory in ASia (REAS) version 2.1 (Kurokawa et al., 2013)
168 is a regional emission inventory for Asia, including monthly emissions of most major air
169 pollutants, e.g., black carbon (BC), organic carbon (OC), sulfur dioxide (SO₂), nitrogen
170 dioxide (NO₂), and greenhouse gases between 2000 and 2008. The spatial resolution of
171 REAS is 0.25×0.25 degrees, covering East, Southeast, South, and Central Asia and the



172 Asian part of Russia (Russian Far East, Eastern and Western Siberia, and the Ural). The
173 area coverage of REAS is from 60°E to 160°E in longitude and from 10°S to 50°N in
174 latitude, which is smaller than our domain configuration. For this reason, we use the
175 Emissions Database for Global Atmospheric Research (EDGAR) version 3.2 (the year 2000
176 emission) (Olivier et al., 2005) and version 4.2 (the year 2005 emission)
177 (<http://edgar.jrc.ec.europa.eu>) to complement the emissions over areas outside REAS
178 coverage. The emission coverage of REAS and EDGAR in our simulated domain is
179 presented in Fig. 1.

180 The Fire INventory from U.S. National Center for Atmospheric Research (NCAR)
181 version 1.5 (FINNv1.5) (Wiedinmyer et al., 2011) is also used in the study to provide fire-
182 based emissions. FINNv1.5 classifies burnings of extra tropical forest, tropical forest
183 (including peatland), savanna, and grassland. The daily data are available from 2002 to
184 2014 with a 1 km spatiotemporal resolution. FINNv1.5 emission inventory also includes the
185 major chemical species (e.g., BC, OC, SO₂, CO, and NO₂) from biomass burning. A
186 modified plume rise algorithm in WRF-Chem, specifically for tropical peat fire, is described
187 in Lee et al. (2017).

188 Compared to fossil fuel emissions, biomass burning emissions vary in space and time
189 (Fig. S1). However, regarding long-term impact, both emissions are important to regional
190 air quality in Southeast Asia (Table 2). BC from biomass burning emissions, for example,
191 has significant inter-annual and inter-seasonal variabilities due to the Southeast Asia
192 monsoon and the El Niño-Southern Oscillation (ENSO) (Lee et al., 2017; Reid et al., 2012),
193 but total BC emissions are equally contributed by fossil fuel and biomass burning sources
194 (Table 2).



195 2.4 Numerical experiment design

196 Three numerical simulations are proposed to investigate the impacts of fire and non-fire
197 aerosols on regional air quality and visibility in Southeast Asia. Among these three runs, the
198 fossil fuel emissions only (FF) simulation and the biomass burning emissions only (BB)
199 simulation are designed to assess the impact of stand-alone non-fire and fire aerosols,
200 respectively. The simulation combining both fossil fuel and biomass burning emissions
201 (FFBB) is to demonstrate the impacts of both types of aerosols; it is also closer to real world
202 case than the two other runs. Based on available years of emission inventories, each of these
203 runs lasts 7 years (i.e., from 2002 to 2008).

204 2.5 Deriving “Low Visibility Day” (LVD) caused by particulate pollution

205 According to Visscher (2013), a visibility reading lower than 10 km is considered a
206 moderate to heavy air pollution event by particulate matter. As in Lee et al. (2017), we
207 define a “low visibility day (LVD)” when the daily-mean surface visibility is lower or equal
208 to 10 km. The modeled visibility is calculated based on the extinction coefficient of the
209 externally mixed aerosols, including BC, OC, sulfate (SO_4^{2-}) and nitrate (NO_3^-), as a
210 function of particle size, by assuming a log-normal size distribution of Aitken and
211 accumulation modes. Note that all these calculations are computed for the wavelength of
212 550 nm. To make the calculated visibility of the modeled aerosols better match the reality,
213 we have also considered the hygroscopic growth of OC, sulfate, and nitrate in the
214 calculation based on the modeled relative humidity (Kiehl et al., 2000; Lee et al., 2017).

215 Our focus in this study is to first identify LVDs and then to determine whether fire or
216 non-fire aerosols alone, or in combination, could cause the occurrence of these LVDs. As a
217 reference, the observed low visibility days were identified and the annual frequency in every



218 year for a given city were also derived by using the GSOD visibility data. Then, the
219 modeled low visibility days were derived following the same procedure. Using these results
220 and based on the logical chart in Fig. 2, the major particulate source (FF, BB or FFBB) that
221 caused the occurrence of observed LVDs were determined. Here, Type 1 LVD represents
222 the cases where either fire or non-fire aerosols alone can cause the observed LVD to occur.
223 Type 2 means that non-fire aerosols are the major contributor to the observed LVD. Type 3
224 is the same as Type 2 but caused by fire aerosols. Type 4 represents the cases where the
225 observed LVD is induced by coexisting fire and non-fire aerosols. The observed LVDs that
226 the model cannot capture are classified as Type 5.

227 2.6 Air Quality Index (AQI)

228 The Air Quality Index is established mainly for the purpose to provide easily
229 understandable information about air pollution to the public. The original derivation of AQI
230 in the U.S. is based on six pollutants: particulate matter (PM₁₀), fine particulate matter
231 (PM_{2.5}), sulfur dioxide (SO₂), carbon monoxide (CO), ozone (O₃), and nitrogen dioxide
232 (NO₂). Each pollutant is scored on a scale extending from 0 through 500 based on the
233 corresponding breakpoints, and then the highest AQI value is reported to the public. In this
234 study, we focus on the AQI derived from modeled 24-hr PM_{2.5} and 9-hr O₃. Note that the
235 original AQI is derived by using 8-hr O₃. Due to the 3-hr output interval of simulated O₃,
236 we use the 9-hr O₃ level instead in this study. An index I_p for pollutant p is calculated by
237 using a segmented linear function that relates pollutant concentration, C_p :

$$238 \quad I_p = \frac{I_{Hi} - I_{Lo}}{B_{Hi} - B_{Lo}} (C_p - B_{Lo}) + I_{Lo}, \quad (1)$$

239 where B_{Hi} is the upper breakpoint of C_p sat category and B_{Lo} is the bottom breakpoint of C_p
240 sat category in Table 3. I_{Hi} and I_{Lo} are the AQI values corresponding to B_{Hi} and B_{Lo} ,



241 respectively. For example, when the 24h-hr $PM_{2.5}$ concentration is $20 \mu g m^{-3}$, B_{Hi} , B_{Lo} , I_{Hi} ,
242 and I_{Lo} are 12, 1, 35.4, 51 and 100, respectively. Then, we selected 24-hr $PM_{2.5}$ and the
243 maximum 9-hr O_3 AQI value in one day to represent daily AQI for $PM_{2.5}$ ($AQI_{(PM_{2.5})}$) and O_3
244 ($AQI_{(O_3)}$), respectively.

245 2.7 Health Impact Assessment (HIA)

246 Previous observations have revealed significantly higher $PM_{2.5}$ concentrations in the
247 cities of Southeast Asia than those in America and Europe (WHO, 2016), implying that the
248 concentration-response functions (CRFs) derived from the latter places may not be directly
249 applicable to Southeast Asia. In this study, we adapted CRFs in Gu and Yim (2016) to
250 estimate the annual number of premature mortalities due to ambient $PM_{2.5}$ concentration in
251 the corresponding region. The relative risk (RR) of four causes of death, including chronic
252 obstructive pulmonary disease, ischemic heart disease, lung cancer, and stroke, when
253 compared with annual incident rate, have been assessed separately. Such risks were
254 described by a log-linear relationship with the corresponding $PM_{2.5}$ concentration level
255 (Burnett et al., 2014). The basic form of RR formulas is provided as follows:

$$256 \quad RR = 1 + \alpha \cdot \left\{ 1 - \exp \left[-\beta (X_j - X_0)^\delta \right] \right\}, \quad (2)$$

257 where X_j and X_0 are the particulate pollutant concentrations ($\mu g m^{-3}$) in the target cities and
258 the threshold value below which no additional risk is assumed to exist, respectively. Here
259 we present the uncertainty range of threshold value between $5.8 \mu g m^{-3}$ and $8.8 \mu g m^{-3}$ in a
260 triangular distribution, as suggested by the GBD 2010 project (Lim et al., 2013).
261 Epidemiological results are not always available in Southeast Asia. To capture both
262 climbing and flattening out phases of CRFs curves suitable for Southeast Asia region, we



263 fitted parameters α , β , and δ in CRFs by the epidemiological samples in the East Asian cities
264 based on Gu and Yim (2016) for China, where $PM_{2.5}$ concentration has a comparable level
265 to that in Southeast Asia.

266 The form of integrated CRF is calculated by the following formula:

$$267 \quad E = \sum_j (RR_j - 1) / RR_j \cdot P_j \cdot f_j, \quad (3)$$

268 where P refers to the population in the researched cities from 2002 to 2008, retrieved from
269 statistics in their respective countries (DSM, 2010; NSCB, 2009; NSOT, 2010; CSOM,
270 2010; GSOV, 2009; DSS, 2008, 2016; NISC, 2013; BPS, 2009). f denotes the baseline
271 incident rate above 30 years of age (WHO, 2017).

272 **3 Results**

273 **3.1 Model evaluation**

274 Multiple ground-based observations are used in this study to evaluate the model's
275 performance particularly in simulating aerosol and major gaseous chemical species such as
276 ozone and carbon monoxide. $PM_{2.5}$ observations in Southeast Asia are very limited,
277 especially for the modeling period of this study. Therefore, PM_{10} concentrations derived
278 from AQI in Kuala Lumpur (Malaysia) are used to present the variation of particulate matter
279 during haze and non-haze seasons. Comparing with the observations, the model accurately
280 predicted PM_{10} concentration, especially during haze seasons (July to October) (Fig. 3a),
281 however, it produced a systematic negative bias of $20 \mu\text{g m}^{-3}$ in background PM_{10}
282 concentration during non-haze periods. This discrepancy between modeled and observed
283 background PM_{10} concentration could come from either the relatively coarse resolution of
284 the model or the underestimation of aerosol or aerosol precursor emissions, or both. Philip



285 et al. (2017) indicated that most global emission inventories do not include anthropogenic
286 fugitive, combustion, and industrial dust (AFCID) from urban sources, typically including
287 fly ash from coal combustion and industrial processes (e.g. iron and steel production, cement
288 production), resuspension from paved and unpaved roads, mining, quarrying, and
289 agricultural operations, and road-residential-commercial construction. In their study, they
290 estimated a 2–16 $\mu\text{g m}^{-3}$ increase in fine particulate matter ($\text{PM}_{2.5}$) concentration across
291 East and South Asia simply by including AFCID emission. In addition to PM_{10} data, we
292 have also used observed visibility to evaluate model performance. As mentioned in Sect.
293 2.5, the modeled visibility values are derived from the extinction coefficient of the
294 externally mixed aerosols and simulated fine particulate concentrations. As shown in Fig. 4,
295 the model correctly predicted about 40% observed low-visibility events during the fire
296 seasons, while 60% miss-captured low-visibility events are mainly due to the missing
297 AFCID. The details of this are discussed in Sect. 4.1. On the other hand, the model has
298 overestimated the visibility range for many cases with observed visibility lower than 7 km.
299 Such an underestimate is likely due to the 36-km model resolution used in the study, which
300 could be too coarse to resolve the typical size of air plumes containing high concentration of
301 fine particulate matters.

302 The observed CO and O₃ levels in the only WMO GAW station in the region, Bukit
303 Kototabang, Indonesia (West Sumatra) are used to evaluate the model performance in
304 simulating gas phase chemistry. Fossil fuel and biomass combustions and biogenic
305 emissions are among the major sources of CO in the region, while O₃ production is mainly
306 resulted from photochemical reactions of precursors such as nitrogen oxides, volatile
307 organic compounds, and CO, largely from anthropogenic emissions. Due to its geographic
308 location, the primary source of CO in Bukit Kototabang is from biomass burning, and high



309 CO levels hence occur during fire seasons (Fig. 3b). The model accurately captured
310 observed CO levels during the simulation. Model simulated evolution of volume mixing
311 ratio of O₃ also very well matches observations, though with a positive bias of about 20
312 ppbv on average (34.8 ± 10.1 versus 13.4 ± 6.1 ppbv) (Fig. 3c).

313 **3.2 Fire- and non-fire-caused LVDs in four selected cities and over the whole** 314 **Southeast Asia**

315 By comparing the annual mean PM_{2.5} concentration in 50 Association of Southeast
316 Asian Nations (ASEAN) cities between three simulations, we identify that there are 13
317 ASEAN cities receiving more than 70% PM_{2.5} concentration from non-fire sources, while
318 there are 10 ASEAN cities where fire aerosols are the major (more than 70%) component of
319 PM_{2.5} (Fig. 5). Note that although fire aerosols are the major component of annual mean
320 PM_{2.5} concentration in these 10 ASEAN cities, the influence period of fire aerosols normally
321 is only about 3 to 5 months. The rest of the ASEAN cities are essentially influenced by
322 coexisting fire and non-fire aerosols. Note that the sum of PM_{2.5} concentrations in FF and
323 BB is not necessarily equal to the PM_{2.5} concentration in FFBB in any given city due to non-
324 linearity in modeled aerosol processes.

325 Based on the logical chart shown in Fig. 2, we can use the modeled results to classify
326 observed LVDs into 5 types of events with different main aerosol sources. In Bangkok,
327 there are about 165 ± 14 LVDs ($45 \pm 4\%$) per year during 2002-2008 based on observations.
328 Modeled results suggest that about 60% of these LVDs can be brought by either fire or non-
329 fire aerosols (the sum of Type 1, Type 2, and Type 3 in Fig. 2; see Table 4). Generally
330 speaking, fire and non-fire aerosols contribute equally towards the haze events occurring in
331 Bangkok. A more interesting finding is that $11 \pm 4\%$ of LVDs need a combination of both



332 fire and non-fire aerosols to occur (Type 4). This highlights the importance of fire aerosols
333 in worsening air quality of otherwise moderate haze conditions under the existing suspended
334 non-fire aerosols. Overall, the model missed about $29\pm 5\%$ of LVDs of Bangkok during the
335 simulation period.

336 Haze occurs slightly less frequently in Kuala Lumpur than Bangkok. There are about
337 104 ± 51 LVDs ($29\pm 14\%$) per year in Kuala Lumpur during 2002-2008. Thirty-six percent of
338 these LVDs are caused by either fire or non-fire aerosols; while $15\pm 6\%$ of the LVDs need a
339 combination of both aerosol sources to form haze (Table 4). Our study shows that non-fire
340 aerosols are capable of causing of 28% of LVDs occurring in Kuala Lumpur, even in the
341 absence of fire aerosols. Once we include the impact of fire aerosols, the model can capture
342 an additional 23% of LVDs, of which most are Type 4 case. Overall, fire and non-fire
343 aerosols make similar contributions to observed LVDs in Kuala Lumpur.

344 In Singapore, there are about 50 ± 14 LVDs ($14\pm 4\%$) per year during 2002-2008. The
345 contribution of non-fire aerosols to LVDs is about 8%. Compared to the additional 25% of
346 LVDs owing to fire aerosols, the contribution of non-fire aerosols to LVDs is small in
347 Singapore. However, the model failed to capture a high percentage of LVD cases in both
348 Kuala Lumpur ($49\pm 26\%$) and Singapore ($67\pm 21\%$) (Type 5; see Table 4). As discussed in
349 Sect. 3.1, missing AFCID in the emission inventory could explain why the model failed to
350 capture the LVDs in these two sites. Further discussion is presented in Sect. 4.1.

351 The annual mean LVDs among 50 ASEAN cities is 192 ± 8 days ($53\pm 2\%$) during 2002-
352 2008. Applying the logical chart described in Fig. 2 to analyze cases of each of these
353 ASEAN cities, we find that by considering aerosols emitted from non-fire emissions alone,
354 about 59% of observed LVDs can be explained, whereas considering fire aerosols adds an
355 additional 13% of LVDs. Conversely, by considering aerosols emitted from fire along,



356 about 47% of observed LVDs can be explained, whereas adding non-fire aerosols adds an
357 additional 25% of LVDs. Two-eight percent of observed LVDs remains unexplained. In
358 general, non-fire aerosols appear to be the major contributor to LVDs in these cities.

359 **3.3 Impacts of ozone and PM_{2.5} on air quality and human health**

360 Similar to PM_{2.5}, O₃ also brings public concerns health besides air quality (Chen et al.,
361 2007). Previously, in Sect. 3.1, we have discussed that the model systematically
362 overestimated O₃ volume mixing ratio by 20 ppbv comparing to observations.
363 Overestimated 9-hr O₃ will lead to a mistakenly derived high AQI_(O₃). Nevertheless, the
364 relative differences of AQI_(O₃) between various model simulations can still provide useful
365 information of the relative contributions of fire and non-fire emissions, either alone or in
366 combination, on air quality and potentially human health.

367 We find that modeled 9-hr O₃ in Bangkok from non-fire emissions (FF) alone triggered
368 19% of daily AQI_(O₃) to reach moderate and unhealthy pollution level during 2002-2008,
369 while fire emissions (BB) alone can only trigger 3% of such situation (Table 5). In
370 comparison, combining fire and non-fire emissions as derived from the simulation of FFBB
371 can cause 33% of daily AQI_(O₃) to reach moderate and unhealthy pollution level. In Kuala
372 Lumpur and Singapore, O₃ is not the major source for air quality degradation, where fire or
373 non-fire emissions alone can seldom cause O₃ levels to reach even moderate pollution
374 levels. For example, in the FF simulation, only 5% of daily AQI_(O₃) readings in Kuala
375 Lumpur and 1% in Singapore reached moderate pollution levels. Again, the majority of the
376 high AQI_(O₃) cases result from combining fire and non-fire emissions (FFBB) (Table 5).
377 Overall, non-fire emissions alone only cause 6% of daily AQI_(O₃) to reach moderate
378 pollution levels in 50 ASEAN cities, whereas about 12% of moderate and unhealthy
379 pollution cases resulted from the combined effect of fire and non-fire emissions.



380 We find that in Southeast Asia, $PM_{2.5}$ actually plays a more important role than O_3 in
381 causing high AQI cases. In Bangkok, $PM_{2.5}$ resulted in 37% and 33% high daily $AQI_{(PM_{2.5})}$
382 cases FF and BB simulation, respectively (Table 6). Among these, three times more cases
383 with daily $AQI_{(PM_{2.5})}$ reaching unhealthy levels can be attributed to $PM_{2.5}$ from BB than
384 those from FF (Table 6). However, the unhealthy levels caused by fire aerosols alone still
385 occur relatively infrequently in Bangkok, Kuala Lumpur and Singapore. In Bangkok, a city
386 with an 8 million population, persistent aerosol emissions from non-fire sources, aided by
387 seasonal fire aerosols, cause almost two-thirds of daily air quality readings to reach
388 moderate or unhealthy pollution levels. Kuala Lumpur and Singapore also have 48% and
389 22% bad air quality days during 2002-2008, respectively (Table 6). Examining 24-hr $PM_{2.5}$
390 $AQI_{(PM_{2.5})}$ among 50 ASEAN cities shows that non-fire aerosols alone contribute to
391 moderate to unhealthy pollution levels 2.6 times more often than fire aerosols alone (23%
392 versus 9%). Compared to the modeled results in FF, $PM_{2.5}$ in FFBB increases 10% more
393 bad air quality to moderate and unhealthy pollution level (Table 6). This result is consistent
394 with the findings in Sect. 3.2.

395 We have examined the health impacts due to $PM_{2.5}$ in 50 ASEAN cities using the
396 method described in Sect. 2.7 and the results show that the top three cities for premature
397 mortality caused by particulate pollution are Jakarta (Indonesia), Bangkok (Thailand), and
398 Hanoi (Vietnam) with 910, 1076, and 624 premature mortalities per year, respectively (Fig.
399 6). The premature mortality in Jakarta is mainly due to exposure to $PM_{2.5}$ particles emitted
400 from non-fire emissions (95%), the same situation as in Hanoi (80%). However, in
401 Bangkok, the health impact due to fire and non-fire aerosols are equally critical (Figs. S2
402 and S3). In general, owing to the increasing trend of non-fire emissions during the analysis
403 period, the premature mortalities due to $PM_{2.5}$ emitted from non-fire sources have increased



404 with time in most ASEAN cities (Fig. S2). Besides this, higher fire aerosols levels in
405 Sumatra and Borneo in 2002, 2004 and 2006 also increased the number of premature
406 mortalities in cities such as Kuching, which were exposed to particulate matters from these
407 burning events (Figs. 6 and S3).

408 **3.4 The impact of fire and non-fire aerosols on regional climate**

409 Besides influencing surface and air temperature through scattering and absorbing solar
410 radiation, aerosols can also alter the spatiotemporal patterns of precipitation via aerosol
411 direct and indirect effects (Wang, 2015). Over the modeled domain, rainfall (in quantity)
412 mainly comes from convective clouds. When the model is configured with a relatively
413 coarse resolution as adopted in our study, however, the convective precipitation process is
414 calculated through the cumulus parameterization of the model, which follows a mass-flux
415 approach to diagnose rainfall and does not interact with aerosols. Despite of this drawback,
416 aerosols can still influence the radiation budget through their direct effect. The
417 thermodynamic consequences of this effect can further influence the cloud formation. On
418 the other hand, the model does contain aerosol-cloud microphysical interaction for
419 stratiform clouds; therefore, aerosols can influence these clouds through the so-called
420 indirect effects by providing cloud condensation nuclei for cloud droplets to form. Hence,
421 cumulus rainfall can be still affected indirectly through dynamical and thermodynamic
422 processes initiated by either aerosol direct effects, indirect effects in stratiform clouds, or
423 both.

424 By comparing the precipitation in FF and FFBB, we have examined the impact of the
425 extra forcing from fire aerosols on precipitation in the modeled Southeast Asia domain
426 (10°S-20°N in latitude, 90°E-150°E in longitude). Non-fire aerosols provide a baseline
427 pattern because of the persistency of fossil fuel emissions, while biomass burning emissions



428 load additional aerosols in the air to alter total aerosol radiative forcing, which then would
429 change precipitation. Through aerosol direct and indirect effects, the difference of monthly
430 regional mean downward shortwave radiation at surface is $8.8 \pm 4.3 \text{ W m}^{-2}$ ($232.6 \pm 19.0 \text{ W m}^{-2}$
431 2 in FF versus $223.8 \pm 20.1 \text{ W m}^{-2}$ in FFBB; Fig. S4). The data are calculated over land only.
432 Owing to the reduction of surface incoming solar radiation by fire aerosols, surface skin
433 temperature is $0.2 \pm 0.2 \text{ K}$ lower in FFBB than in FF (Fig. S5). Lower surface temperature
434 brought by fire aerosols would suppress convection (Berg et al., 2013). As a result, the
435 model produced a lower monthly regional mean precipitation in FFBB than in FF by 0.2 ± 0.4
436 mm day^{-1} over land ($11.15 \pm 4.27 \text{ mm day}^{-1}$ versus $11.35 \pm 4.42 \text{ mm day}^{-1}$; Fig. 7), with the
437 most significant rainfall changes occurring in the fire emission regions of Sumatra and
438 Borneo. We also find higher cloud water mass in FFBB, which has stronger radiative
439 forcing than aerosols. Nevertheless, further study using a cloud-resolving resolution is
440 necessary.

441 **4 Discussion**

442 **4.1 Uncertainty of emission inventory**

443 In this study, we have noticed the simulated $\text{PM}_{2.5}$ concentrations in Singapore are often
444 lower than the observations of the National Environment Agency of Singapore
445 (<https://data.gov.sg/dataset/air-pollutant-particulate-matter-pm2-5>) ($6.1 \mu\text{g m}^{-3}$ versus 20.3
446 $\mu\text{g m}^{-3}$ in annual mean during 2002-2008). Owing to the lower simulated $\text{PM}_{2.5}$
447 concentration in Singapore, the model could not capture many observed LVDs (Table 4) and
448 consequently underestimated AQI levels resulting from $\text{PM}_{2.5}$. As mentioned before, Philip
449 et al. (2017) have pointed out that global atmospheric models can produce a $2\text{--}16 \mu\text{g m}^{-3}$
450 underestimation in fine particulate mass concentration across East and South Asia due to a
451 lack of inclusion of anthropogenic fugitive, combustion and industrial dust emissions in the



452 emission inventories. Most current global emission inventories indeed either do not include
453 anthropogenic fugitive and industrial dusts, or substantially underestimate the quantities of
454 these emissions (Klimont et al., 2016; Janssens-Maenhout et al., 2015). The fugitive dust
455 sources, such as road and construction dust, in most major cities in Southeast Asia are
456 apparently not well represented in the emission inventory used in our study. To correct
457 these systematic underestimates, we have used crustal matter and residual matter from
458 filtered SPARTAN PM_{2.5} measurements as the reference to fill in the modeled PM_{2.5} for the
459 missing anthropogenic dust component. Excluding the high concentration samples during
460 the fire haze events, the mean concentration of crustal matter and residual matter is 25.8 μg
461 m⁻³ in Hanoi, 10.4 μg m⁻³ in Singapore, 18.1 μg m⁻³ in Bandung, and 9.2 μg m⁻³ in Manila.
462 We then added these values as the anthropogenic dust components in modeled aerosol
463 abundance to recalculate modeled visibility and AQI_(PM_{2.5}). Table 7 shows the calculated
464 percentage of LVDs caused by various aerosol types in Fig. 2 before and after the above
465 correction.

466 Adding the anthropogenic dust component based on in-situ measurement in the
467 modeled results can reproduce 98% of observed LVDs in Hanoi (an increase from 79%).
468 Because the missing anthropogenic dusts are included in non-fire aerosols, LVDs in Type 1
469 and Type 2 are heavily weighted in the new result. The results also show the LVDs in
470 Hanoi are mainly caused by non-fire aerosols and the contribution of fire aerosols is
471 relatively small. Adding anthropogenic dust components also reduced the number of
472 missing LVDs events from 67% to 20% in Singapore. Differing from Hanoi, not only Type
473 2 LVDs but also Type 4 LVDs increased after introducing the missing anthropogenic dusts
474 in Singapore, implying that the fire and non-fire aerosols are equally important in causing
475 LVDs there. After applying the correction, non-fire aerosols alone can explain 30% LVDs



476 while coexisting fire and non-fire aerosols can explain 40% LVDs in Singapore (Table 7).
477 Note that the mode of the distribution of observed visibility in Singapore is around 11 km.
478 Therefore, when fire occurs in the surrounding countries, even a moderate addition to the
479 aerosol abundance from fire can worsen visibility to reach a low visibility condition
480 (visibility < 10 km). Because of the poor data quality of observed visibility in Bandung
481 (only less than 10% observations are available), introducing the missing anthropogenic dust
482 did not help to characterize the major aerosol contribution. In Manila, the number of missed
483 LVDs in the model reduced 35% while Type 2 and Type 4 LVDs increased 26% and 9%,
484 respectively, after introducing the missing anthropogenic dusts. Nevertheless, even after
485 adding anthropogenic dusts in non-fire aerosol category, the model still missed 57% of
486 LVDs in Manila. This is mainly because the model did not capture many fire events in that
487 area, likely due to underestimation of fire emissions in the emission inventory.

488 Besides LVDs, the missing anthropogenic dusts also substantially affect the modelled
489 $AQI_{(PM_{2.5})}$. Table 8 shows the frequency of various $AQI_{(PM_{2.5})}$ levels calculated respectively
490 with and without the missing anthropogenic dusts in Hanoi, Singapore, Bandung, and
491 Manila. After considering the missing anthropogenic dusts, modeled air pollution levels in
492 Hanoi and Bandung persistently reach the moderate or unhealthy pollution levels. In
493 Singapore, modeled frequency of moderate and unhealthy cases also increase from 22% to
494 66%, and in Manila from 8% to 36%. Furthermore, the number of premature mortalities in
495 Singapore and Manila increases significantly from 0 to 230 and 128, respectively (Table 9).
496 These results indicate the importance for models to include anthropogenic fugitive and
497 industrial dust in order to capture low visibility events in the region.

498 Model resolution, the accuracy of both fire and non-fire emissions, and other potential
499 aerosol sources all could cause the model bias in capturing observed LVDs and thus



500 underestimate the air pollution levels and associated health impacts. Among those possible
501 factors, the fire and non-fire emission inventories are the most critical. Applying inverse
502 modeling, for example, could optimize the emission inventories and hence improve the
503 model performance.

504 **4.2 Experiment in applying machine learning algorithms to predict the** 505 **occurrence of PM_{2.5} caused LVDs**

506 The severe and frequent LVDs or haze events due to particulate pollution have brought
507 a serious issue to Southeast Asian countries in recent decades, interrupting working and
508 school schedules, transportation, and outdoor activities alongside causing human health
509 issues that all lead to economic loss. One measure to minimize such economic loss is to
510 provide reliable forecasts for the occurrence of LVDs to allow corresponding mitigations be
511 implemented beforehand.

512 Traditional physical models such as WRF-Chem are developed based on fluid
513 dynamics, chemical reactions, and mass conservation equations to link processes on
514 different scales and to predict consequences resulting from circulation and physiochemical
515 process evolutions. However, various parameterizations, and numerical as well as input
516 data errors can all lead to the uncertainty of model prediction. Specifically, for the task of
517 forecasting the occurrence of haze events (i.e., LVDs), using these models is nearly
518 impossible due to the lack of real-time emission estimates to drive aerosol chemical and
519 physical processes. On the other hand, Machine Learning (ML) algorithms permit
520 interpretation of large quantity of complex historical data based on computer analyses, and
521 this capacity of ML seems promising for us to derive suitable conditions for hazes from
522 historical data and hence to forecast the likelihood of the occurrence of such events.



523 Here, we experiment using the so-called supervised learning skill that trains or
524 optimizes a machine to produce the outcomes based on input data (or features) as close as
525 possible to known results, or gaining an accuracy as high as possible. In our experiment, we
526 have applied 6 different ML algorithms, including Nearest Neighbors (Pedregosa et al.,
527 2011), Linear Support Vector Machine (SVM) (Schölkopf and Smola, 2002), SVM with
528 Radial Basis Function Kernel (non-linear SVM) (Scholkopf et al., 1997; Quinlan, 1986),
529 Decision Tree (Quinlan, 1986), Random Forest (Breiman, 2001), and Neural Network
530 (Haykin et al., 2009), to reproduce past visibility patterns or to predict haze occurrence.
531 Through the supervised learning procedure, we have also examined the importance of each
532 input variable. These ML machines are trained for predicting LVDs at three airports in
533 Singapore reporting to the GSOD, i.e., Changi, Seletar, and Paya Labar. All the input data
534 or features are listed in Table S3. Data are available from 2000 to 2015 at Changi and Paya
535 Labar but only between 2004 and 2015 at Seletar.

536 We have used several different classifications in the training. The first one uses two
537 classes, corresponding to haze (visibility lower or equal to 10 km) and non-haze (visibility
538 higher than 10 km) events. Another applied 2-class classification uses 7 km instead of 10
539 km in identifying the haze events. In addition, a 3-class classification has also been tested,
540 which includes two haze classes: visibility lower than 7 km and between 10 and 7 km,
541 respectively. The training-testing ratio was set to be 60:40. In comparison, the highest
542 validation accuracy and F_1 -score (Powers, 2011) in any algorithm appear in the machine for
543 Changi site, while the difference in accuracy between each algorithm is small (Figs. 8 and
544 9). However, the accuracy for each algorithm at Seletar and Paya Labar drops dramatically
545 by about 20-30% in 2-class classification using 10-km visibility and 3-class classification.
546 The reason for the best performances in Changi is likely to be the least frequency of haze



547 events at this site (account for only 10% of the total LVDs), in comparison, 37% and 44% of
548 haze events occurred at Paya Labar and Seletar during the training time period, respectively.
549 The model also predicts non-haze events with higher accuracy than haze events at Changi.
550 Using severe haze (visibility < 7 km) instead of moderate haze (visibility < 10 km) to label
551 haze event can also increase accuracy (over 80%). This could be due to fact that severe haze
552 events are primarily caused by heavy biomass burnings, whose occurrence would be well
553 captured in the satellite hotspot input data.

554 Besides accuracy and F_1 -score analysis, we have also used the *feature importance*
555 function in scikit-learn Random Forest package to measure the importance of various
556 features (i.e. Gini importance) (Pedregosa et al., 2011). The function takes array of features
557 and computes the normalized total reduction of the criterion brought by that feature. The
558 higher the value, the more important the feature is to the forecasting machine. We find that
559 the hotspot counts from three fire regions are ranked consistently among the top three most
560 important features for most model predictions in all three classifications (Fig. 10; Fig. S6
561 and S7). The values of importance of hotspot counts are higher than 0.15. Analysis also
562 suggests that “Month” is among the top five most important features in all models, followed
563 by wind direction and relative humidity (Fig. 10), implying that besides fire hotspot,
564 seasonal monsoon wind patterns, wind-related weather conditions (i.e., SRV in Fig. 10) are
565 also important factors in forecasting the occurrence of haze events in Singapore. In
566 addition, relative humidity is a critical variable for visibility (i.e., growth of hygroscopic
567 particles can drastically enhance the light extinction). These results are consistent with
568 previous studies of haze events in Singapore (Reid et al., 2012; Lee et al., 2017). To our
569 surprise, precipitation in the fire regions does not appear to have a significant impact on
570 Singapore haze compared to other features.



571 **5 Summary**

572 We have quantified the impacts of fire (emitted from biomass burning) and non-fire
573 (emitted from anthropogenic sources other than biomass burning) aerosols on air quality and
574 visibility degradation over Southeast Asia, by using WRF-Chem in three scenarios driven
575 respectively by aerosol emissions from: (a) fossil fuel burning only, (b) biomass burning
576 only, and (c) both fossil fuel and biomass burning. Based on the results from these
577 scenarios, we conclude that the major reason behind the occurrence of observed low
578 visibility days (LVDs) in 50 ASEAN cities is aerosols from non-fire anthropogenic sources
579 (59%), while fire aerosols cause an additional 13% of LVDs (both alone and coexisting with
580 non-fire aerosols) in these cities. Conversely, by considering aerosols emitted from fire
581 along, about 47% of observed LVDs can be explained, whereas adding non-fire aerosols
582 adds an additional 25% of LVDs. Out of these results, model fails to capture about 28% of
583 observed LVDs. Our results show that owing to the economic growth in Southeast Asia,
584 non-fire aerosols have become the major reason to cause LVDs in most Southeast Asian
585 cities. However, for certain cities including Singapore, LVDs are likely caused by
586 coexisting fire and non-fire aerosols. Hence, both fire and non-fire emissions play important
587 roles in visibility degradation in Southeast Asia.

588 Furthermore, we have also used air quality index or AQI derived from modeled 9-hr O₃
589 and 24-hr PM_{2.5} to analyze the air quality of these 50 ASEAN cities. The results are
590 consistent with the visibility modeling and analysis, indicating that PM_{2.5} particles, primarily
591 those from non-fire emissions, are the major reason behind high AQI_(PM_{2.5}) occurrence in
592 these Southeast Asian cities. In addition to non-fire PM_{2.5} stand-alone cases, coexisting fire
593 and non-fire PM_{2.5} jointly caused an increase of 11% in bad air quality events with moderate
594 polluted or unhealthy pollution levels (23% versus 34%). The premature mortality among



595 the analyzed ASEAN cities has increased from ~4110 in 2002 to ~6540 in 2008. Bangkok
596 (Thailand), Jakarta (Indonesia), and Hanoi (Vietnam) are the top three cities in our analysis
597 for premature mortality due to air pollution, with 1076, 910, and 624 premature mortalities
598 per year, respectively.

599 We find the reason behind the model's miss-capturing of 28% observed LVDs averaged
600 over 50 ASEAN cities is largely due to a lack of inclusion of anthropogenic fugitive and
601 industrial as well as road dust from urban sources in the emission inventories used in this
602 study. Using filtered $PM_{2.5}$ data from the SPARTAN stations in Hanoi, Singapore, Bandung,
603 and Manila to filled the missing aerosol components from these excluded sources can
604 drastically increase model captured LVDs in these cities, for example, by 47% in Singapore.
605 The improvement in LVD prediction is especially substantial in non-fire aerosols alone
606 cases (Type 2; from 5% to 25%) and coexisting fire and non-fire aerosols cases (Type 4;
607 from 14% to 40%). Including anthropogenic dusts in modeled results also increases the
608 occurrence of cases with moderate and unhealthy air pollution levels from 22% to 66% in
609 Singapore. Our study clearly demonstrates the importance of anthropogenic dust along with
610 other fugitive industrial and urban sources in air quality and visibility degradation in certain
611 Southeast Asian cities such as Singapore.

612 We have also experimented using machine learning algorithms to predict the occurrence
613 of LVDs caused by $PM_{2.5}$. Six different machine learning algorithms have been applied,
614 including Nearest Neighbors, Linear Support Vector Machine (SVM), SVM with Radial
615 Basis Function Kernel (non-linear SVM), Decision Tree, Random Forest, and Neural
616 Network. The effort is on forecasting hazes in three GSOD sites in Singapore. We find that
617 the machine learning algorithms can predict severe haze events (visibility < 7 km) with an



618 accuracy greater than 80% in any station. On the other hand, the accuracy is found to be
619 sensitive to the selection of features, labelling of outcome, and forecast sites.

620 The current study extends our previous effort (Lee et al., 2017) by using a model
621 including a full chemistry and aerosol package instead of a smoke aerosol module without
622 chemistry. The added model capacity provides more complete quantitative description of
623 physiochemical processes that allow us to better analyze the contribution of fire versus non-
624 fire aerosols to the regional air quality and visibility degradation. Our results show that the
625 majority of the population in Southeast Asian cities are exposed to air pollution that can be
626 mostly attributed to non-fire aerosols. On the other hand, our analysis also suggests that for
627 certain cities such as Singapore, severe air pollution are likely caused by coexisting fire and
628 non-fire aerosols. All these further complicate the options for air pollution mitigation.

629 **6 Data availability**

630 FINNv1.5 emission data are publicly available from
631 <http://bai.acom.uar.edu/Data/fire/>. REAS and EDGAR emission data can be
632 downloaded from <https://www.nies.go.jp/REAS/> and
633 <http://edgar.jrc.ec.europa.eu/overview.php?v=42>, respectively. Malaysia API records
634 can be obtained from http://apims.doe.gov.my/public_v2/home.html. The observational
635 visibility from the GSOD can be downloaded from [https://data.noaa.gov/dataset/global-](https://data.noaa.gov/dataset/global-surface-summary-of-the-day-gsod)
636 [surface-summary-of-the-day-gsod](https://data.noaa.gov/dataset/global-surface-summary-of-the-day-gsod). CO and O₃ in WHO GAW station can be obtained
637 from <http://ds.data.jma.go.jp/gmd/wdcgg/>. Fine particle data from SPARTAN are
638 publicly available in <http://spartan-network.weebly.com/>. WRF-Chem simulated data are
639 available upon request from Hsiang-He Lee (hsiang-he@smart.mit.edu).

640



641 **Acknowledgements**

642 This research was supported by the National Research Foundation Singapore through the
643 Singapore-MIT Alliance for Research and Technology, the interdisciplinary research
644 program of Center for Environmental Sensing and Modeling. It was also supported by the
645 U.S. National Science Foundation (AGS-1339264) and U.S. Department of Energy (DE-
646 FG02-94ER61937). The authors thank MIT Greater China Fund for Innovation 2015 for
647 facilitating the collaboration between the Chinese University of Hong Kong and MIT
648 research teams. The authors would like to acknowledge the Ministry of Natural Resources
649 and Environment, Department of Environment, Malaysia for making Malaysia Air Pollution
650 Index data available; the World Meteorology Organization (WMO) Global Atmosphere
651 Watch (GAW) station Bukit Kototabang, SPARTAN, NCEP-FNL, and NCAR FINN
652 working groups for releasing their data to the research communities; and the NCAR WRF
653 developing team for providing the numerical model for this study. The computational work
654 for this article was performed on resources of the National Supercomputing Centre,
655 Singapore (<https://www.nscg.sg>).

656

657

658

659 **References**

- 660 Ackermann, I. J., Hass, H., Memmesheimer, M., Ebel, A., Binkowski, F. S., and Shankar, U.:
661 Modal aerosol dynamics model for Europe: development and first applications,
662 Atmospheric Environment, 32, 2981-2999, [http://dx.doi.org/10.1016/S1352-
663 2310\(98\)00006-5](http://dx.doi.org/10.1016/S1352-2310(98)00006-5), 1998.
664 Benjamini, Y., and Hochberg, Y.: Controlling the False Discovery Rate: A Practical and
665 Powerful Approach to Multiple Testing, Journal of the Royal Statistical Society.
666 Series B (Methodological), 57, 289-300, 1995.



- 667 Berg, P., Moseley, C., and Haerter, J. O.: Strong increase in convective precipitation in
668 response to higher temperatures, *Nature Geosci*, 6, 181-185,
669 [http://www.nature.com/ngeo/journal/v6/n3/abs/ngeo1731.html -](http://www.nature.com/ngeo/journal/v6/n3/abs/ngeo1731.html-supplementary-information)
670 [supplementary-information](http://www.nature.com/ngeo/journal/v6/n3/abs/ngeo1731.html-supplementary-information), 2013.
- 671 BPS: Statistik Indonesia-Statistical Yearbook of Indonesia, Badan Pusat Statistik, 2009.
- 672 Breiman, L.: Random Forests, *Machine Learning*, 45, 5-32, 10.1023/A:1010933404324,
673 2001.
- 674 Burnett, R. T., Pope III, C. A., Ezzati, M., Olives, C., Lim, S. S., Mehta, S., Shin, H. H., Singh,
675 G., Hubbell, B., and Brauer, M.: An integrated risk function for estimating the
676 global burden of disease attributable to ambient fine particulate matter
677 exposure, *Environmental health perspectives*, 122, 397, 2014.
- 678 Chen, T.-M., Kuschner, W. G., Gokhale, J., and Shofer, S.: Outdoor air pollution: ozone
679 health effects, *The American journal of the medical sciences*, 333, 244-248,
680 2007.
- 681 Crippa, P., Castruccio, S., Archer-Nicholls, S., Lebron, G. B., Kuwata, M., Thota, A., Sumin,
682 S., Butt, E., Wiedinmyer, C., and Spracklen, D. V.: Population exposure to
683 hazardous air quality due to the 2015 fires in Equatorial Asia, *Scientific Reports*,
684 6, 37074, 10.1038/srep37074, 2016.
- 685 CSOM: Statistical Yearbook 2010, The Government of the Republic of the Union of
686 Myanmar, 2010.
- 687 DSM: Population distribution and basic demographic characteristics, Department of
688 Statistics, Malaysia, Malaysia, 2010.
- 689 DSS: Singapore's Resident Population, 2003-2007, Department of Statistics Singapore,
690 Singapore, 2008.
- 691 DSS: Population Trends 2016, Department of Statistics Singapore, Singapore, 2016.
- 692 Frankenberg, E., McKee, D., and Thomas, D.: Health consequences of forest fires in
693 Indonesia, *Demography*, 42, 109-129, 10.1353/dem.2005.0004, 2005.
- 694 GSOV: Population and Employment, General Statistics Office Of Vietnam, 2009.
- 695 Gu, Y., and Yim, S. H. L.: The air quality and health impacts of domestic trans-boundary
696 pollution in various regions of China, *Environment International*, 97, 117-124,
697 <http://dx.doi.org/10.1016/j.envint.2016.08.004>, 2016.
- 698 Haykin, S. S., Haykin, S. S., Haykin, S. S., and Haykin, S. S.: *Neural networks and learning*
699 *machines*, Pearson Upper Saddle River, NJ, USA:, 2009.
- 700 IEA: Energy and Climate Change, World Energy Outlook Special Report, International
701 Energy Agency, pp. 74 -77, 2015.
- 702 Janssens-Maenhout, G., Crippa, M., Guizzardi, D., Dentener, F., Muntean, M., Pouliot, G.,
703 Keating, T., Zhang, Q., Kurokawa, J., Wankmüller, R., Denier van der Gon, H.,
704 Kuenen, J. J. P., Klimont, Z., Frost, G., Darras, S., Koffi, B., and Li, M.: HTAP_v2.2: a
705 mosaic of regional and global emission grid maps for 2008 and 2010 to study
706 hemispheric transport of air pollution, *Atmos. Chem. Phys.*, 15, 11411-11432,
707 10.5194/acp-15-11411-2015, 2015.
- 708 Kiehl, J. T., Schneider, T. L., Rasch, P. J., Barth, M. C., and Wong, J.: Radiative forcing due
709 to sulfate aerosols from simulations with the National Center for Atmospheric
710 Research Community Climate Model, Version 3, *Journal of Geophysical*
711 *Research: Atmospheres*, 105, 1441-1457, 10.1029/1999JD900495, 2000.
- 712 Klimont, Z., Kupiainen, K., Heyes, C., Purohit, P., Cofala, J., Rafaj, P., Borken-Kleefeld, J.,
713 and Schöpp, W.: Global anthropogenic emissions of particulate matter including



- 714 black carbon, Atmos. Chem. Phys. Discuss., 2016, 1-72, 10.5194/acp-2016-880,
715 2016.
- 716 Kunii, O., Kanagawa, S., Yajima, I., Hisamatsu, Y., Yamamura, S., Amagai, T., and Ismail, I.
717 T. S.: The 1997 Haze Disaster in Indonesia: Its Air Quality and Health Effects,
718 Archives of Environmental Health: An International Journal, 57, 16-22,
719 10.1080/00039890209602912, 2002.
- 720 Kurokawa, J., Ohara, T., Morikawa, T., Hanayama, S., Janssens-Maenhout, G., Fukui, T.,
721 Kawashima, K., and Akimoto, H.: Emissions of air pollutants and greenhouse
722 gases over Asian regions during 2000–2008: Regional Emission inventory in
723 ASia (REAS) version 2, Atmos. Chem. Phys., 13, 11019-11058, 10.5194/acp-13-
724 11019-2013, 2013.
- 725 Lee, H. H., Bar-Or, R. Z., and Wang, C.: Biomass burning aerosols and the low-visibility
726 events in Southeast Asia, Atmos. Chem. Phys., 17, 965-980, 10.5194/acp-17-
727 965-2017, 2017.
- 728 Li, Y., Henze, D. K., Jack, D., Henderson, B. H., and Kinney, P. L.: Assessing public health
729 burden associated with exposure to ambient black carbon in the United States,
730 Science of The Total Environment, 539, 515-525,
731 <https://doi.org/10.1016/j.scitotenv.2015.08.129>, 2016.
- 732 Lim, S. S., Vos, T., Flaxman, A. D., Danaei, G., Shibuya, K., Adair-Rohani, H., AlMazroa, M.
733 A., Amann, M., Anderson, H. R., and Andrews, K. G.: A comparative risk
734 assessment of burden of disease and injury attributable to 67 risk factors and
735 risk factor clusters in 21 regions, 1990–2010: a systematic analysis for the
736 Global Burden of Disease Study 2010, The lancet, 380, 2224-2260, 2013.
- 737 Malaysia, D. o. E.: A Guide To Air Pollutant Index in Malaysia, 4 ed., edited by: Malaysia,
738 D. o. E., 18 pp., 2000.
- 739 Marlier, M. E., DeFries, R. S., Voulgarakis, A., Kinney, P. L., Randerson, J. T., Shindell, D.
740 T., Chen, Y., and Faluvegi, G.: El Nino and health risks from landscape fire
741 emissions in southeast Asia, Nature Clim. Change, 3, 131-136,
742 [http://www.nature.com/nclimate/journal/v3/n2/abs/nclimate1658.html -
743 supplementary-information](http://www.nature.com/nclimate/journal/v3/n2/abs/nclimate1658.html-supplementary-information), 2013.
- 744 Miettinen, J., Shi, C., and Liew, S. C.: Deforestation rates in insular Southeast Asia
745 between 2000 and 2010, Global Change Biology, 17, 2261-2270,
746 10.1111/j.1365-2486.2011.02398.x, 2011.
- 747 National Centers for Environmental Prediction, N. W. S. N. U. S. D. o. C.: NCEP FNL
748 Operational Model Global Tropospheric Analyses, continuing from July 1999,
749 10.5065/D6M043C6, 2000.
- 750 NISC: Cambodia Inter-censal Population Survey 2013-Final Report, National Institute
751 of Statistics, Ministry of Planning, Phnom Penh, Cambodia, 2013.
- 752 NSCB: 2009 Philippine Statistical Yearbook, National Statistical Coordination Board,
753 Philippine 2009.
- 754 NSOT: Population and Housing Census 2010, National Statistical Office of Thailand,
755 2010.
- 756 Olivier, J., Van Aardenne, J., Dentener, F., Ganzeveld, L., and JAHW, P.: Recent trends in
757 global greenhouse gas emissions: regional trends and spatial distribution of key
758 sources.(169Kb) In: " Non-CO 2 Greenhouse Gases (NCGG-4)", A. van Amstel
759 (coord.), Millpress, Rotterdam, ISBN, 90, 043, 2005.



- 760 Pedregosa, F., Varoquaux, G., Gramfort, A., Michel, V., Thirion, B., Grisel, O., Blondel, M.,
761 Prettenhofer, P., Weiss, R., and Dubourg, V.: Scikit-learn: Machine learning in
762 Python, *Journal of Machine Learning Research*, 12, 2825-2830, 2011.
- 763 Philip, S., Martin, R. V., Snider, G., Weagle, C. L., Donkelaar, A. v., Brauer, M., Henze, D. K.,
764 Klimont, Z., Venkataraman, C., Sarath, K. G., and Zhang, Q.: Anthropogenic
765 fugitive, combustion and industrial dust is a significant, underrepresented fine
766 particulate matter source in global atmospheric models, *Environmental
767 Research Letters*, 12, 044018, 2017.
- 768 Powers, D. M.: Evaluation: from precision, recall and F-measure to ROC, informedness,
769 markedness and correlation, *Journal of Machine Learning Technologies*, 2, 37-
770 63, 2011.
- 771 Quinlan, J. R.: Induction of decision trees, *Machine learning*, 1, 81-106, 1986.
- 772 Reid, J. S., Xian, P., Hyer, E. J., Flatau, M. K., Ramirez, E. M., Turk, F. J., Sampson, C. R.,
773 Zhang, C., Fukada, E. M., and Maloney, E. D.: Multi-scale meteorological
774 conceptual analysis of observed active fire hotspot activity and smoke optical
775 depth in the Maritime Continent, *Atmos. Chem. Phys.*, 12, 2117-2147,
776 10.5194/acp-12-2117-2012, 2012.
- 777 Schell, B., Ackermann, I. J., Hass, H., Binkowski, F. S., and Ebel, A.: Modeling the
778 formation of secondary organic aerosol within a comprehensive air quality
779 model system, *Journal of Geophysical Research: Atmospheres (1984-2012)*,
780 106, 28275-28293, 2001.
- 781 Scholkopf, B., Sung, K.-K., Burges, C. J., Girosi, F., Niyogi, P., Poggio, T., and Vapnik, V.:
782 Comparing support vector machines with Gaussian kernels to radial basis
783 function classifiers, *IEEE transactions on Signal Processing*, 45, 2758-2765,
784 1997.
- 785 Schölkopf, B., and Smola, A. J.: *Learning with kernels: support vector machines,*
786 *regularization, optimization, and beyond*, MIT press, 2002.
- 787 Smith, A., Lott, N., and Vose, R.: The Integrated Surface Database: Recent Developments
788 and Partnerships, *Bulletin of the American Meteorological Society*, 92, 704-708,
789 doi:10.1175/2011BAMS3015.1, 2011.
- 790 Snider, G., Weagle, C. L., Martin, R. V., van Donkelaar, A., Conrad, K., Cunningham, D.,
791 Gordon, C., Zwicker, M., Akoshile, C., Artaxo, P., Anh, N. X., Brook, J., Dong, J.,
792 Garland, R. M., Greenwald, R., Griffith, D., He, K., Holben, B. N., Kahn, R., Koren, I.,
793 Lagrosas, N., Lestari, P., Ma, Z., Vanderlei Martins, J., Quel, E. J., Rudich, Y., Salam,
794 A., Tripathi, S. N., Yu, C., Zhang, Q., Zhang, Y., Brauer, M., Cohen, A., Gibson, M. D.,
795 and Liu, Y.: SPARTAN: a global network to evaluate and enhance satellite-based
796 estimates of ground-level particulate matter for global health applications,
797 *Atmos. Meas. Tech.*, 8, 505-521, 10.5194/amt-8-505-2015, 2015.
- 798 Snider, G., Weagle, C. L., Murdymootoo, K. K., Ring, A., Ritchie, Y., Stone, E., Walsh, A.,
799 Akoshile, C., Anh, N. X., Balasubramanian, R., Brook, J., Qonitan, F. D., Dong, J.,
800 Griffith, D., He, K., Holben, B. N., Kahn, R., Lagrosas, N., Lestari, P., Ma, Z., Misra,
801 A., Norford, L. K., Quel, E. J., Salam, A., Schichtel, B., Segev, L., Tripathi, S., Wang,
802 C., Yu, C., Zhang, Q., Zhang, Y., Brauer, M., Cohen, A., Gibson, M. D., Liu, Y.,
803 Martins, J. V., Rudich, Y., and Martin, R. V.: Variation in global chemical
804 composition of PM_{2.5}: emerging results from SPARTAN, *Atmos. Chem. Phys.*, 16,
805 9629-9653, 10.5194/acp-16-9629-2016, 2016.



- 806 Stockwell, W. R., Kirchner, F., Kuhn, M., and Seefeld, S.: A new mechanism for regional
807 atmospheric chemistry modeling, *Journal of Geophysical Research:*
808 *Atmospheres*, 102, 25847-25879, 10.1029/97JD00849, 1997.
- 809 van der Werf, G. R., Morton, D. C., DeFries, R. S., Olivier, J. G. J., Kasibhatla, P. S., Jackson,
810 R. B., Collatz, G. J., and Randerson, J. T.: CO₂ emissions from forest loss, *Nature*
811 *Geosci*, 2, 737-738,
812 http://www.nature.com/ngeo/journal/v2/n11/supinfo/ngeo671_S1.html,
813 2009.
- 814 Visscher, A. D.: *Air Dispersion Modeling: Foundations and Applications*, First ed., John
815 Wiley & Sons, Inc., 2013.
- 816 Wang, C.: A modeling study on the climate impacts of black carbon aerosols, *Journal of*
817 *Geophysical Research: Atmospheres*, 109, n/a-n/a, 10.1029/2003JD004084,
818 2004.
- 819 Wang, C.: Impact of direct radiative forcing of black carbon aerosols on tropical
820 convective precipitation, *Geophysical Research Letters*, 34,
821 10.1029/2006GL028416, 2007.
- 822 Wang, C.: Anthropogenic aerosols and the distribution of past large-scale precipitation
823 change, *Geophysical Research Letters*, 42, 10,876-810,884,
824 10.1002/2015GL066416, 2015.
- 825 Wiedinmyer, C., Akagi, S. K., Yokelson, R. J., Emmons, L. K., Al-Saadi, J. A., Orlando, J. J.,
826 and Soja, A. J.: The Fire INventory from NCAR (FINN): a high resolution global
827 model to estimate the emissions from open burning, *Geosci. Model Dev.*, 4, 625-
828 641, 10.5194/gmd-4-625-2011, 2011.
- 829 Wilks, D. S.: "The Stippling Shows Statistically Significant Grid Points": How Research
830 Results are Routinely Overstated and Overinterpreted, and What to Do about It,
831 *Bulletin of the American Meteorological Society*, 97, 2263-2273,
832 10.1175/BAMS-D-15-00267.1, 2016.
- 833
- 834



835

Table 1. WRF physics scheme configuration

836

Physics Processes	Scheme
microphysics	Morrison (2 moments) scheme
longwave radiation	RRTMG scheme
shortwave radiation	RRTMG scheme
surface-layer	MYNN surface layer
land surface	Unified Noah land-surface model
planetary boundary layer	MYNN 2.5 level TKE scheme
cumulus parameterization	Grell-Freitas ensemble scheme

837

838



839

840 Table 2. Mean annual emissions of BC, OC, SO₂, CO and NO₂ from biomass burning
841 emission (BB; from FINN emission inventory) and fossil fuel burning emission (FF; from
842 the combination of REAS and EDGAR emission inventories shown in Fig. 1) in the
843 simulated domain from 2002 to 2008. Parentheses show the percentage of emission from
844 fire and non-fire sources.

845

Units: Tg/yr	BC	OC	SO₂	CO	NO₂
BB	0.4 (50%)	4.1 (73%)	0.4 (7%)	71.6 (64%)	2.6 (37%)
FF	0.4 (50%)	1.4 (27%)	5.8 (93%)	39.9 (36%)	4.3 (63%)

846

847



848 Table 3. Comparison of the Air Quality Index (AQI) values with level of pollution index
849 category and breakpoints for AQI derived from modeled 24-hr PM_{2.5} (µg m⁻³) and modeled
850 9-hr O₃ (ppb).
851

Index Category	AQI	24-hr PM _{2.5} (µg/m ³)	9-hr O ₃ (ppb)
Good	0 - 50	0.0 - 12.0	0 - 59
Moderate	51 - 100	12.1 - 35.4	60 - 75
Unhealthy	101 - 200	35.5 - 150.4	76 - 115
Very Unhealthy	201 - 300	150.5 - 250.4	116 - 374
Hazardous	301 - 400	250.5 - 350.4	/
Hazardous	401 - 500	350.5 - 500.4	/

852

853



854 Table 4. The contribution of fire aerosols (BB), non-fire aerosols (FF), or coexisting
855 aerosols (FFBB) to low visibility days (LVDs) (based on the logic chart in Fig. 2) in
856 Bangkok, Kuala Lumpur, Singapore, and among 50 Association of Southeast Asian Nations
857 (ASEAN) cities during 2002-2008
858

	Bangkok	Kuala Lumpur	Singapore	50 ASEAN cities
FF∩BB (Type 1)	22±10%	12±5%	3±4%	39±5%
FF (Type 2)	19±5%	16±16%	5±4%	20±3%
BB (Type 3)	19±7%	8±5%	11±13%	8±2%
FF+BB (Type 4)	11±4%	15±6%	14±8%	5±1%
Missing (Type 5)	29±5%	49±26%	67±21%	28±2%

859

860



861 Table 5. The frequency of occurrence of air pollution level in Bangkok, Kuala Lumpur,
 862 Singapore, and 50 Association of Southeast Asian Nations (ASEAN) cities derived using 9-
 863 hr Ozone (O_3) volume mixing ratio in FF, BB, and FFBB during 2002-2008
 864

Bangkok	AQI(O_3)	FF	BB	FFBB
Good	0-50	81±3%	97±1%	69±3%
Moderate	51-100	17±2%	3±1%	21±3%
Unhealthy	101-200	2±1%	0±0%	11±1%
Very Unhealthy	201-300	0±0%	0±0%	0±0%
Hazardous	301-400	0±0%	0±0%	0±0%
Hazardous	401-500	0±0%	0±0%	0±0%
Kuala Lumpur	AQI(O_3)	FF	BB	FFBB
Good	0-50	95±2%	100±1%	83±6%
Moderate	51-100	5±2%	0±1%	15±5%
Unhealthy	101-200	0±0%	0±0%	2±1%
Very Unhealthy	201-300	0±0%	0±0%	0±0%
Hazardous	301-400	0±0%	0±0%	0±0%
Hazardous	401-500	0±0%	0±0%	0±0%
Singapore	AQI(O_3)	FF	BB	FFBB
Good	0-50	99±1%	100±0%	94±3%
Moderate	51-100	1±1%	0±0%	5±2%
Unhealthy	101-200	0±0%	0±0%	1±1%
Very Unhealthy	201-300	0±0%	0±0%	0±0%
Hazardous	301-400	0±0%	0±0%	0±0%
Hazardous	401-500	0±0%	0±0%	0±0%
50 ASEAN cities	AQI(O_3)	FF	BB	FFBB
Good	0-50	94±1%	99±0%	88±2%
Moderate	51-100	6±1%	1±0%	10±2%
Unhealthy	101-200	0±0%	0±0%	2±0%
Very Unhealthy	201-300	0±0%	0±0%	0±0%
Hazardous	301-400	0±0%	0±0%	0±0%
Hazardous	401-500	0±0%	0±0%	0±0%

865

866

867 Table 6. Same as Table 5 but using 24-hr PM_{2.5} concentration

868

Bangkok	AQI_(PM2.5)	FF	BB	FFBB
Good	0-50	63±6%	67±5%	38±2%
Moderate	51-100	34±5%	24±3%	45±3%
Unhealthy	101-200	3±2%	9±4%	17±4%
Very Unhealthy	201-300	0±0%	0±0%	0±0%
Hazardous	301-400	0±0%	0±0%	0±0%
Hazardous	401-500	0±0%	0±0%	0±0%
Kuala Lumpur	AQI_(PM2.5)	FF	BB	FFBB
Good	0-50	73±3%	78±8%	52±7%
Moderate	51-100	27±4%	18±6%	40±4%
Unhealthy	101-200	0±0%	4±3%	8±4%
Very Unhealthy	201-300	0±0%	0±0%	0±0%
Hazardous	301-400	0±0%	0±0%	0±0%
Hazardous	401-500	0±0%	0±0%	0±0%
Singapore	AQI_(PM2.5)	FF	BB	FFBB
Good	0-50	92±5%	92±4%	78±5%
Moderate	51-100	8±4%	6±2%	19±4%
Unhealthy	101-200	0±1%	1±2%	3±2%
Very Unhealthy	201-300	0±0%	0±0%	0±0%
Hazardous	301-400	0±0%	0±0%	0±0%
Hazardous	401-500	0±0%	0±0%	0±0%
50 ASEAN cities	AQI_(PM2.5)	FF	BB	FFBB
Good	0-50	77±1%	90±3%	66±3%
Moderate	51-100	19±1%	7±2%	26±2%
Unhealthy	101-200	4±0%	2±1%	8±2%
Very Unhealthy	201-300	0±0%	0±0%	0±0%
Hazardous	301-400	0±0%	0±0%	0±0%
Hazardous	401-500	0±0%	0±0%	0±0%

869



870 Table 7. The old (without anthropogenic dust) and new (with anthropogenic dust in FF and
 871 FFBB) calculated percentage of observed low visibility days (LVDs) caused by defined
 872 aerosol types in Fig. 2 in Hanoi, Singapore, Bandung and Manila during 2002-2008.
 873

	Hanoi		Singapore		Bandung		Manila	
	old	new	old	new	old	new	old	new
FF∩BB (Type 1)	38±32%	40±31%	3±4%	5±7%	41±73%	41±74%	0±0%	1±1%
FF (Type 2)	34±8%	57±13%	5±4%	25±13%	8±19%	8±20%	3±3%	29±33%
BB (Type 3)	2±2%	0±0%	11±13%	9±10%	0±0%	0±0%	3±3%	2±3%
FF+BB (Type 4)	5±3%	1±1%	14±8%	40±19%	0±0%	0±0%	2±2%	11±3%
Missing (Type 5)	21±15%	2±4%	67±21%	20±9%	51±56%	51±57%	92±41%	57±16%

874
 875



876

877

878

879

880

Table 8. The frequency of various daily air pollution levels in Hanoi, Singapore, Bandung and Manila derived using 24-hr $PM_{2.5}$ concentration with (new) and without (old) the missing anthropogenic dusts in FFBB during 2002-2008.

Hanoi	AQI_(PM_{2.5})	old	new
Good	0-50	43±7%	0±0%
Moderate	51-100	46±3%	32±4%
Unhealthy	101-200	10±3%	67±4%
Very Unhealthy	201-300	0±0%	0±0%
Hazardous	301-400	0±0%	0±0%
Hazardous	401-500	0±0%	0±0%
Singapore	AQI_(PM_{2.5})	old	new
Good	0-50	78±5%	33±8%
Moderate	51-100	19±4%	59±8%
Unhealthy	101-200	3±2%	7±3%
Very Unhealthy	201-300	0±0%	0±0%
Hazardous	301-400	0±0%	0±0%
Hazardous	401-500	0±0%	0±0%
Bandung	AQI_(PM_{2.5})	old	new
Good	0-50	36±7%	0±0%
Moderate	51-100	58±5%	52±8%
Unhealthy	101-200	6±3%	48±8%
Very Unhealthy	201-300	0±0%	0±0%
Hazardous	301-400	0±0%	0±0%
Hazardous	401-500	0±0%	0±0%
Manila	AQI_(PM_{2.5})	old	new
Good	0-50	92±4%	64±5%
Moderate	51-100	7±3%	34±5%
Unhealthy	101-200	1±1%	2±1%
Very Unhealthy	201-300	0±0%	0±0%
Hazardous	301-400	0±0%	0±0%
Hazardous	401-500	0±0%	0±0%

881



882 Table 9. Updated $\text{PM}_{2.5}$ concentration ($\mu\text{g m}^{-3}$) and premature mortality (95% confidence
883 intervals) in Hanoi, Singapore, Bandung and Manila with missing anthropogenic dusts.
884

City	$\text{PM}_{2.5}$ ($\mu\text{g m}^{-3}$)	Premature mortality
Hanoi	41.07	671 (210-1184)
Singapore	16.43	230 (22-551)
Bandung	33.18	261 (65-481)
Manila	12.38	128 (12-260)

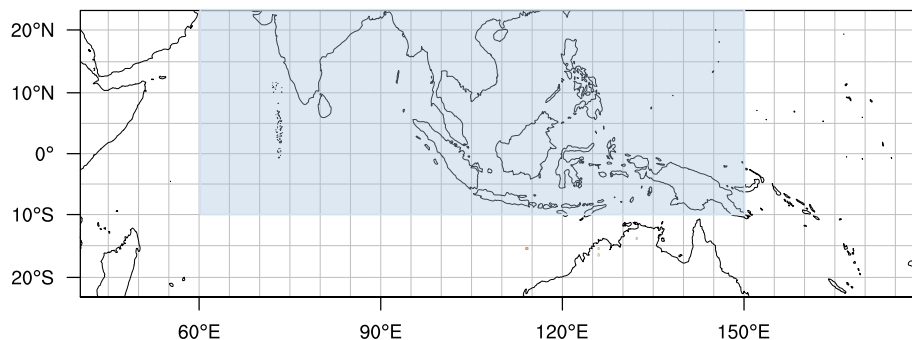
885



886

887

888



889

890

891

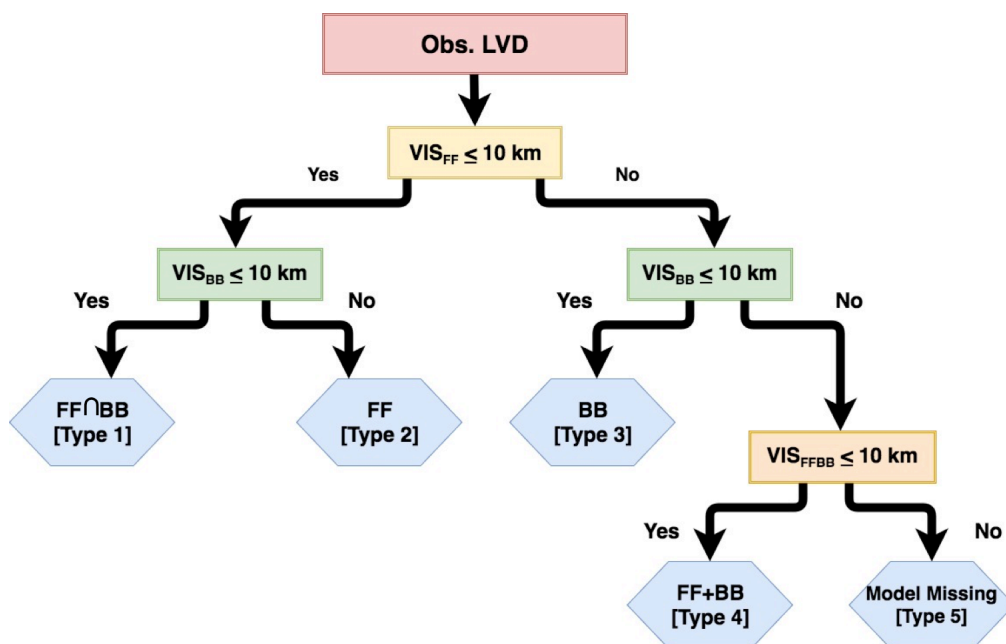
892

893

894

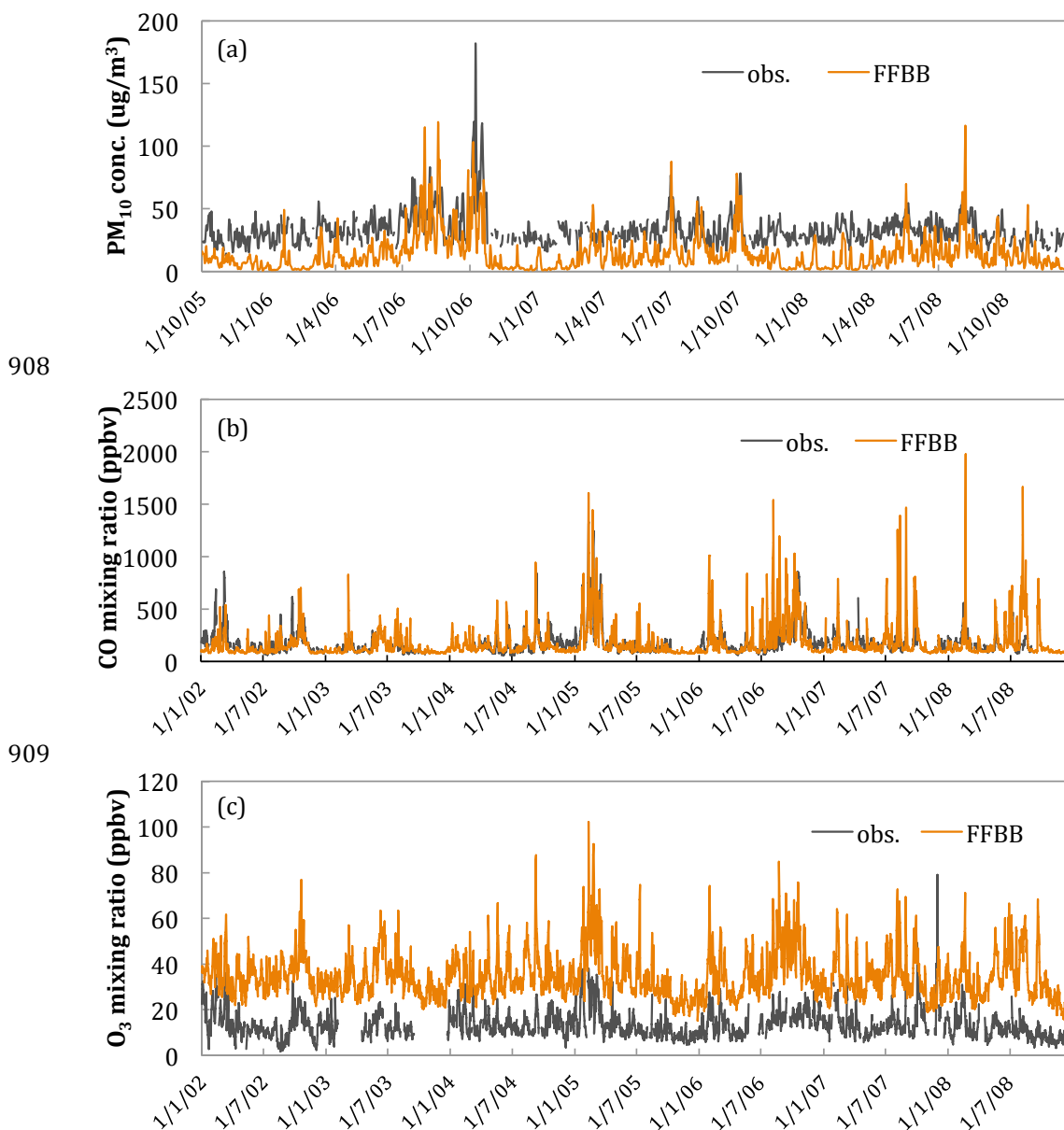
895

Figure 1. Model domain used for simulations. Blue color region indicates the fossil fuel emission coverage from the Regional Emission inventory in ASia (REAS) . The rest of the domain uses the fossil fuel emission from the Emissions Database for Global Atmospheric Research (EDGAR). The domain has 432×148 grid points with a horizontal resolution of 36km.

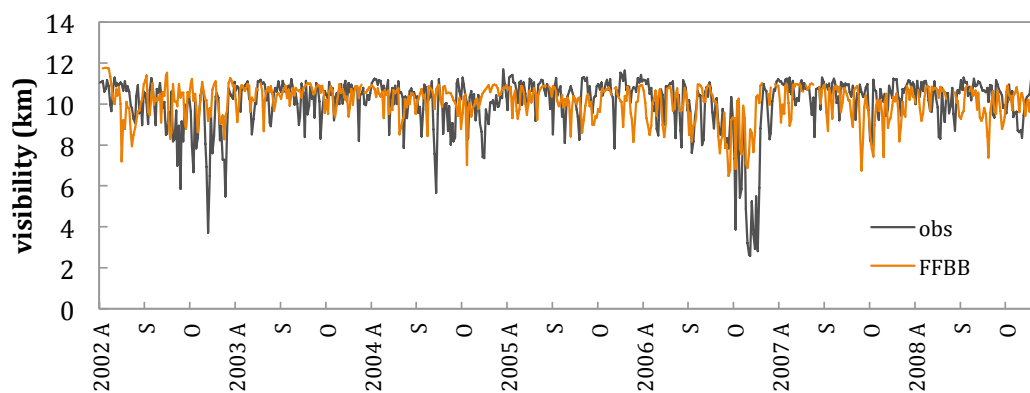


896
 897
 898
 899
 900
 901
 902
 903
 904
 905
 906
 907

Figure 2. Logical chart for fire (BB), non-fire (FF), or coexisting fire and non-fire (FFBB) aerosols caused Low Visibility Day (LVD). “Obs. LVD” is an identified low visibility day from observation. Then, the modeled visibility from FF (VIS_{FF}), BB (VIS_{BB}), and FFBB (VIS_{FFBB}) are used to classify observed LVD into 5 types LVD. Type 1 LVD represents the cases where either fire or non-fire aerosols alone can cause the observed LVD to occur. Type 2 means that non-fire aerosols are the major contributor to the observed LVD. Type 3 means that biomass burning aerosols are the major contributor to the observed LVD. Type 4 represents the cases where the observed LVD is induced by coexisting fire and non-fire aerosols. The observed LVDs that the model cannot capture are classified as Type 5.

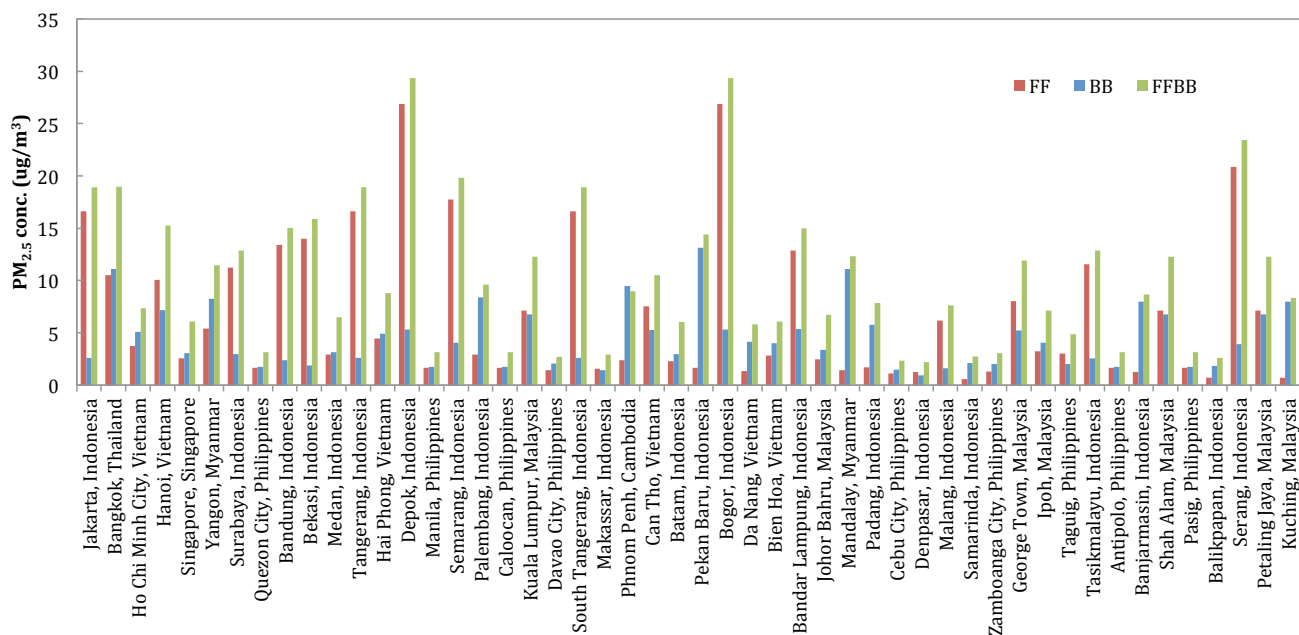


910 Figure 3. (a) Time series of daily surface PM₁₀ ($\mu\text{g m}^{-3}$; AQI derived) from the ground-based
911 observations (black line) and FFBB-simulated results (orange line) in Kuala Lumpur,
912 Malaysia during October 2005 – December 2008. (b) Time series of daily surface CO
913 mixing ratio (ppbv) from the ground-based observations (black line) and FFBB-simulated
914 results (orange line) in Bukit Kototabang, Indonesia during 2002 – 2008. (c) Same as (b) but
915 surface O₃.
916
917



918
919
920
921
922

Figure 4. Comparison of daily visibility between GSOD observation (black line) and FFBB-simulated results (orange line) in Singapore during the fire seasons from 2002 to 2008. A, S, and O in the x axis indicates August, September, and October.



923
924
925
926
927

Figure 5. The annual mean simulated $PM_{2.5}$ concentration ($\mu g m^{-3}$) in 50 Association of Southeast Asian Nations (ASEAN) cities, derived from FF (red), BB (blue), and FFBB (green) simulations and averaged over the period 2002-2008.



928

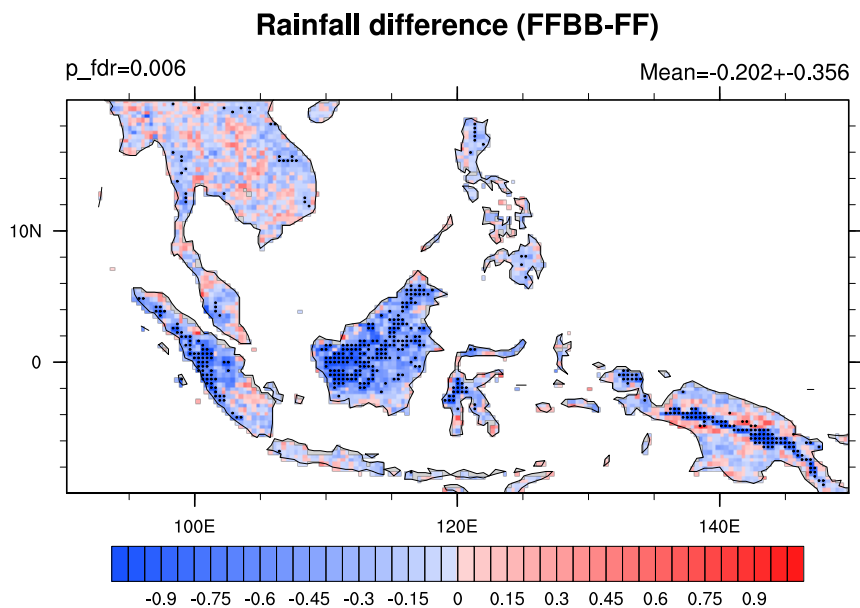
Cities	Country	2002	2003	2004	2005	2006	2007	2008
Jakarta	Indonesia	850 (150-1660)	830 (130-1650)	900 (160-1750)	950 (180-1820)	910 (150-1790)	960 (170-1870)	970 (170-1900)
Bangkok	Thailand	950 (90-1950)	1010 (130-2230)	1030 (130-2280)	1170 (180-2530)	1120 (150-2480)	1180 (160-2590)	1170 (150-2600)
Ho Chi Minh City	Vietnam	0 (0-0)	0 (0-0)	830 (80-1750)	610 (0-1590)	0 (0-1130)	230 (0-1580)	0 (0-1530)
Hanoi	Vietnam	420 (40-880)	520 (80-1020)	540 (80-1060)	560 (90-1100)	570 (80-1120)	610 (100-1190)	1150 (190-2250)
Singapore	Singapore	0 (0-0)	0 (0-0)	0 (0-260)	0 (0-190)	0 (0-290)	0 (0-290)	0 (0-0)
Yangon	Myanmar	0 (0-380)	280 (20-630)	350 (30-730)	330 (30-710)	280 (20-640)	400 (40-820)	330 (20-730)
Surabaya	Indonesia	220 (30-440)	210 (20-430)	230 (30-460)	230 (30-470)	230 (30-470)	240 (30-480)	230 (20-480)
Quezon City	Philippines	0 (0-0)	0 (0-0)	0 (0-0)	0 (0-0)	0 (0-0)	0 (0-0)	0 (0-0)
Bandung	Indonesia	200 (30-400)	200 (30-400)	210 (30-420)	230 (40-450)	200 (20-410)	220 (30-450)	220 (30-440)
Bekasi	Indonesia	150 (20-310)	160 (20-320)	180 (30-350)	190 (30-380)	190 (30-380)	210 (30-410)	210 (30-420)
Medan	Indonesia	0 (0-0)	0 (0-0)	0 (0-230)	10 (0-250)	0 (0-240)	0 (0-160)	0 (0-160)
Tangerang	Indonesia	120 (20-240)	120 (20-250)	140 (20-270)	150 (30-290)	150 (20-300)	170 (30-340)	170 (30-340)
Hai Phong	Vietnam	0 (0-0)	210 (10-480)	200 (0-480)	230 (10-510)	200 (0-500)	270 (30-590)	280 (30-590)
Depok	Indonesia	130 (30-230)	130 (30-250)	150 (30-270)	160 (40-300)	160 (40-310)	180 (40-330)	190 (40-350)
Manila	Philippines	0 (0-0)	0 (0-0)	0 (0-0)	0 (0-0)	0 (0-0)	0 (0-0)	0 (0-0)
Semarang	Indonesia	120 (20-240)	120 (20-240)	140 (30-260)	140 (30-280)	140 (30-280)	150 (30-290)	150 (30-300)
Palembang	Indonesia	100 (10-210)	0 (0-0)	100 (10-210)	0 (0-0)	150 (30-280)	0 (0-0)	0 (0-0)
Caloocan	Philippines	0 (0-0)	0 (0-0)	0 (0-0)	0 (0-0)	0 (0-0)	0 (0-0)	0 (0-0)
Kuala Lumpur	Malaysia	130 (10-290)	100 (0-260)	160 (20-340)	170 (20-360)	170 (20-360)	150 (10-340)	150 (10-340)
Davao City	Philippines	0 (0-0)	0 (0-0)	0 (0-0)	0 (0-0)	0 (0-0)	0 (0-0)	0 (0-0)
South Tangerang	Indonesia	130 (20-250)	120 (20-240)	130 (20-250)	140 (30-260)	130 (20-250)	130 (20-260)	130 (20-260)
Makassar	Indonesia	0 (0-0)	0 (0-0)	0 (0-0)	0 (0-0)	0 (0-0)	0 (0-0)	0 (0-0)
Phnom Penh	Cambodia	0 (0-0)	0 (0-40)	40 (10-90)	30 (0-80)	30 (0-80)	40 (0-90)	40 (0-90)
Can Tho	Vietnam	60 (0-270)	140 (10-310)	180 (20-370)	170 (20-360)	160 (10-350)	180 (20-380)	180 (20-380)
Batam	Indonesia	0 (0-0)	0 (0-0)	0 (0-50)	0 (0-60)	10 (0-80)	0 (0-90)	0 (0-0)
Pekan Baru	Indonesia	20 (0-80)	0 (0-80)	60 (10-120)	80 (20-150)	80 (10-150)	70 (10-140)	70 (10-150)
Bogor	Indonesia	100 (20-180)	100 (20-180)	100 (20-190)	110 (30-200)	110 (20-200)	110 (30-200)	110 (30-210)
Da Nang	Vietnam	0 (0-0)	0 (0-0)	90 (0-210)	0 (0-180)	0 (0-0)	0 (0-170)	0 (0-100)
Bien Hoa	Vietnam	0 (0-0)	0 (0-0)	60 (0-150)	0 (0-130)	0 (0-0)	0 (0-70)	0 (0-100)
Bandar Lampung	Indonesia	70 (10-140)	70 (10-140)	70 (10-140)	70 (10-140)	80 (10-150)	80 (10-150)	80 (10-160)
Johor Bahru	Malaysia	0 (0-0)	0 (0-0)	0 (0-170)	0 (0-160)	0 (0-200)	0 (0-190)	0 (0-70)
Mandalay	Myanmar	0 (0-0)	290 (20-610)	330 (30-670)	300 (30-640)	300 (30-650)	360 (40-740)	340 (30-710)
Padang	Indonesia	0 (0-0)	0 (0-0)	0 (0-60)	0 (0-90)	10 (10-130)	40 (0-110)	30 (0-100)
Cebu City	Philippines	0 (0-0)	0 (0-0)	0 (0-0)	0 (0-0)	0 (0-0)	0 (0-0)	0 (0-0)
Denpasar	Indonesia	0 (0-0)	0 (0-0)	0 (0-0)	0 (0-0)	0 (0-0)	0 (0-0)	0 (0-0)
Malang	Indonesia	30 (0-100)	0 (0-50)	30 (0-100)	20 (0-100)	10 (0-100)	10 (0-100)	0 (0-100)
Samarinda	Indonesia	0 (0-0)	0 (0-0)	0 (0-0)	0 (0-0)	0 (0-0)	0 (0-0)	0 (0-0)
Zamboanga City	Philippines	0 (0-0)	0 (0-0)	0 (0-0)	0 (0-0)	0 (0-0)	0 (0-0)	0 (0-0)
George Town	Malaysia	110 (10-250)	100 (10-240)	140 (10-290)	140 (10-290)	120 (10-270)	120 (10-260)	120 (10-270)
Ipoh	Malaysia	0 (0-0)	0 (0-0)	50 (0-120)	50 (0-120)	0 (0-90)	0 (0-50)	0 (0-90)
Taguig	Philippines	0 (0-0)	0 (0-0)	0 (0-60)	0 (0-0)	0 (0-0)	0 (0-0)	0 (0-0)
Tasikmalayu	Indonesia	30 (0-70)	30 (0-70)	40 (0-80)	40 (10-90)	40 (0-80)	50 (10-90)	50 (10-100)
Antipolo	Philippines	0 (0-0)	0 (0-0)	0 (0-0)	0 (0-0)	0 (0-0)	0 (0-0)	0 (0-0)
Banjarmasin	Indonesia	50 (10-100)	0 (0-0)	50 (10-110)	0 (0-0)	60 (10-110)	0 (0-0)	0 (0-0)
Shah Alam	Malaysia	60 (0-130)	40 (0-110)	70 (10-150)	70 (10-150)	70 (10-150)	60 (0-140)	60 (0-130)
Pasig	Philippines	0 (0-0)	0 (0-0)	0 (0-0)	0 (0-0)	0 (0-0)	0 (0-0)	0 (0-0)
Balikpapan	Indonesia	0 (0-0)	0 (0-0)	0 (0-0)	0 (0-0)	0 (0-0)	0 (0-0)	0 (0-0)
Serang	Indonesia	50 (10-90)	50 (10-90)	50 (10-90)	50 (10-90)	50 (10-90)	50 (10-90)	50 (10-90)
Petaling Jaya	Malaysia	60 (0-120)	40 (0-110)	70 (10-140)	70 (10-140)	70 (10-140)	60 (0-130)	60 (0-130)
Kuching	Malaysia	50 (0-100)	0 (0-0)	50 (0-110)	0 (0-0)	60 (10-130)	0 (0-60)	0 (0-0)

929



930 Figure 6. Premature mortality in different years from 2002 to 2008 and cities in Association of
931 Southeast Asian Nations (ASEAN) due to exposures $PM_{2.5}$ in FFBB (95% confidence intervals).
932 Colors from green to red represent relative number scale.

933



934

935 Figure 7. Total monthly mean precipitation differences (mm day^{-1}) between FFBB and FF
 936 simulations during 2002–2008. Black dot indicates differences that are statistically significant at
 937 a significance level of $\alpha_{\text{fdr}} = 0.05$ after controlling the false discovery rate (FDR) (Benjamini
 938 and Hochberg, 1995; Wilks, 2016). The two-tailed p values are generated by Welch’s t test,
 939 using monthly mean data as the input. The approximate p value threshold, p_fdr, and area mean
 940 and standard deviation (over land only) are written in above the map.

941

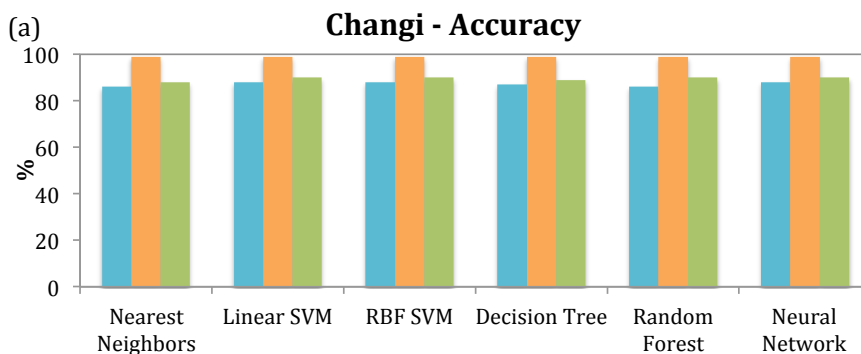
942

943

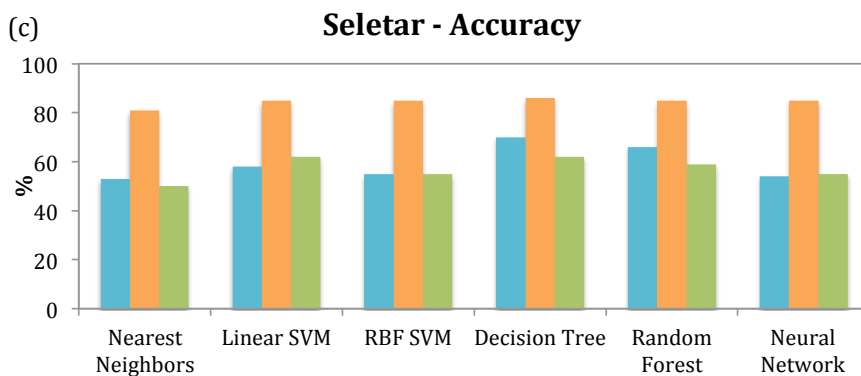
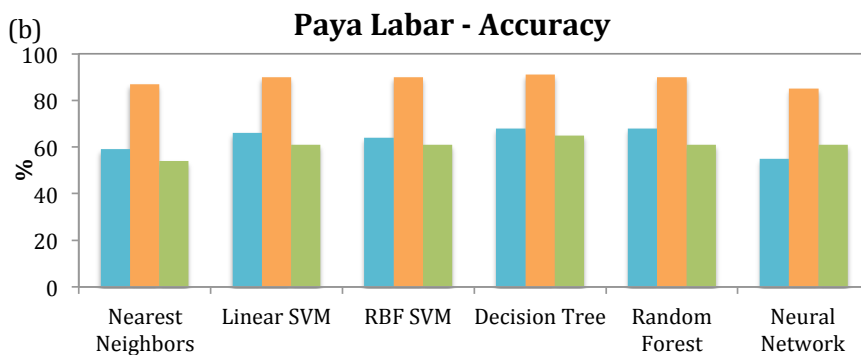
944



945



946



■ 2-class (10 km) ■ 2-class (7 km) ■ 3-class

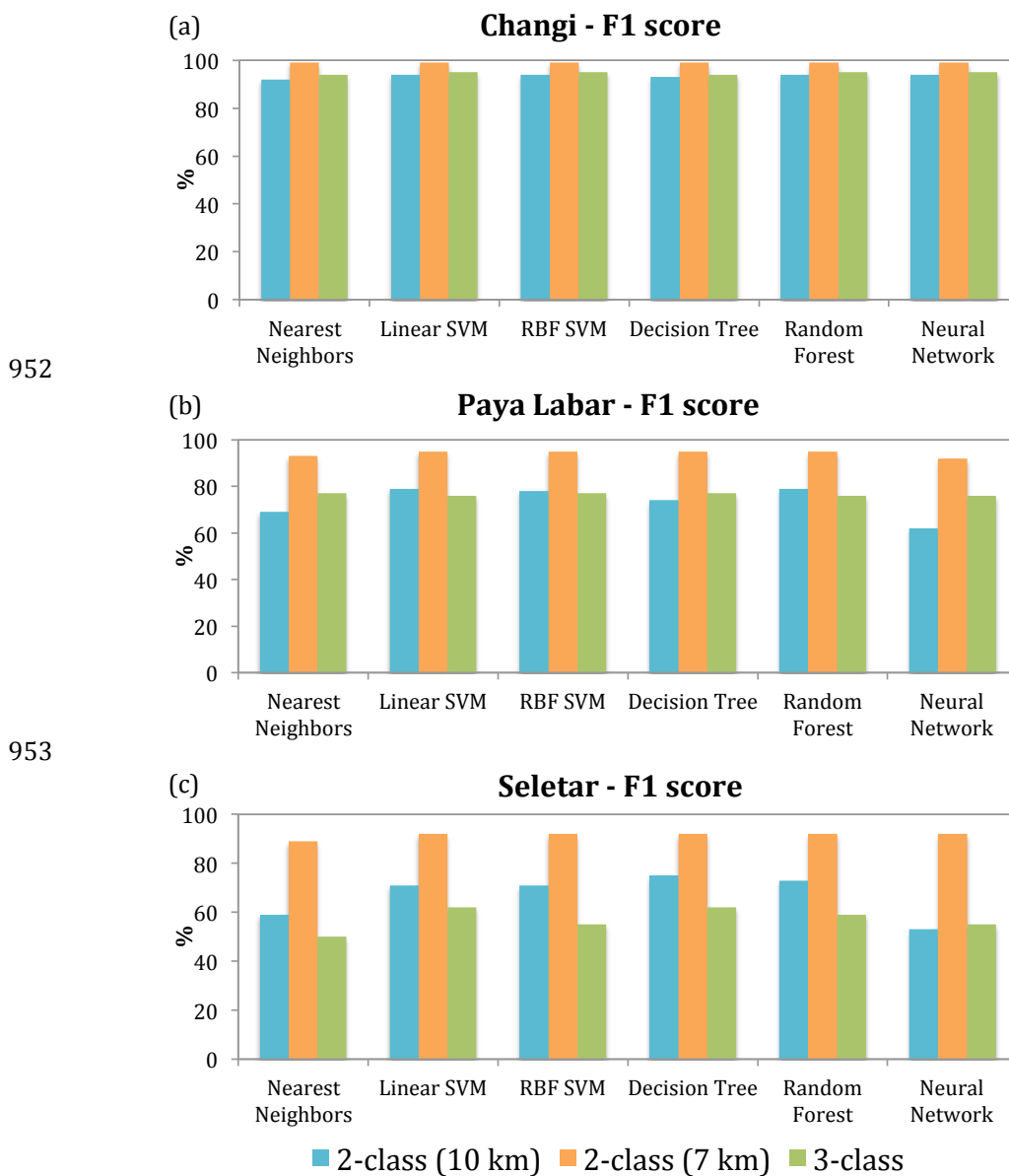
947

948 Figure 8. The testing accuracy in 6 Machine Learning algorithms for two 2-class (7 km or 10

949 km visibility as a breakpoint) and one 3-class classifications haze prediction in (a) Changi, (b)

950 Paya Labar, and (c) Seletar. The units are in percentage.

951



954 Figure 9. The F₁ score in 6 Machine Learning algorithms for two 2-class (7 km or 10 km
955 visibility as a breakpoint) and one 3-class classifications haze prediction in (a) Changi, (b) Paya
956 Labar, and (c) Seletar. The units are in percentage.

958
959

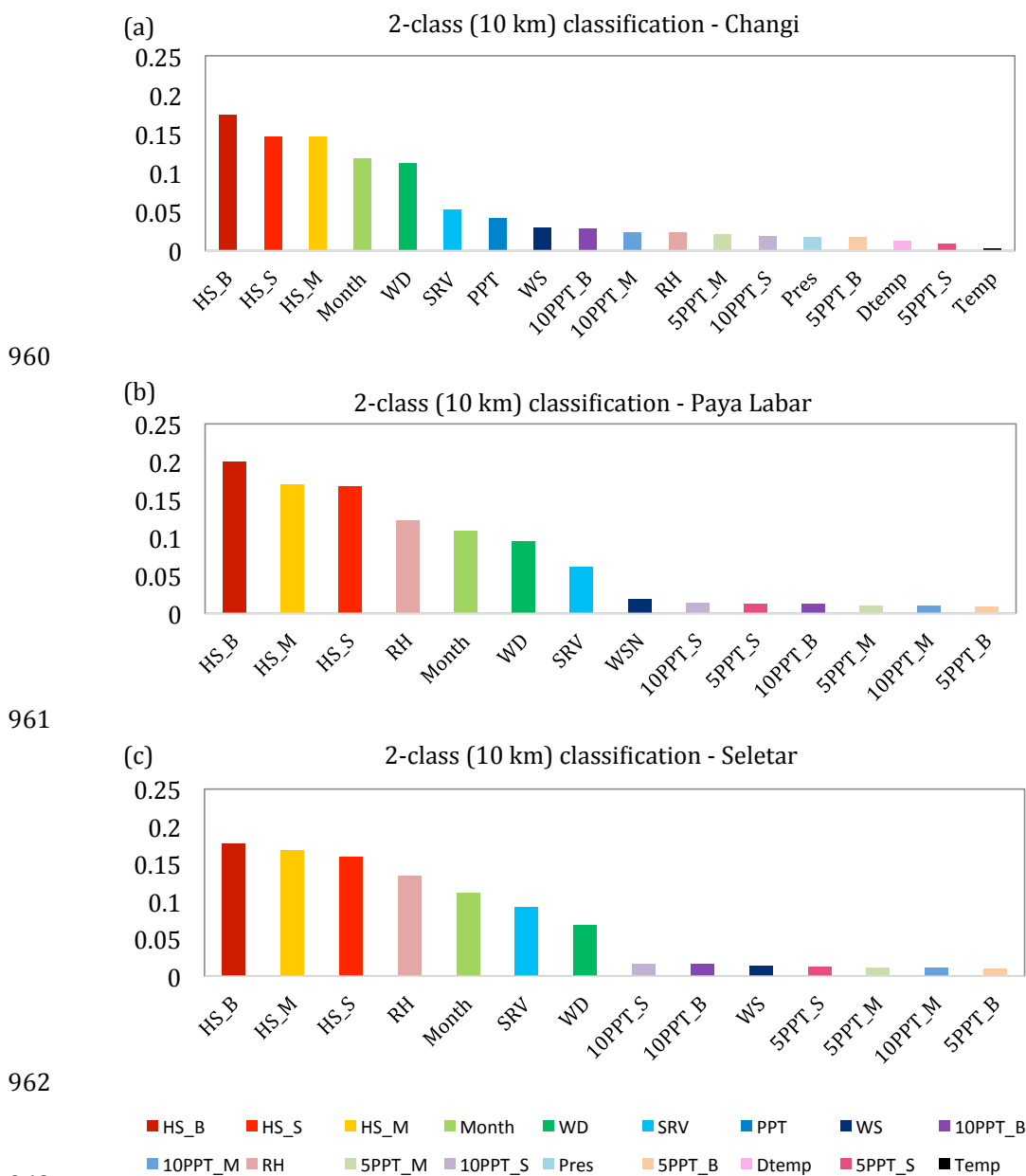


Figure 10. Feature importance by using 2-class classification Random Forest algorithm in (a) Changi, (b) Paya Labar, and (c) Seletar. Desired outputs, haze versus non-haze events, are defined by using visibility 10 km as a breakpoint. Full name of each input feature are listed in Table S3.



971 Benjamini, Y., and Hochberg, Y.: Controlling the False Discovery Rate: A Practical and
972 Powerful Approach to Multiple Testing, *Journal of the Royal Statistical Society. Series B*
973 (Methodological), 57, 289-300, 1995.
974 Wilks, D. S.: “The Stippling Shows Statistically Significant Grid Points”: How Research
975 Results are Routinely Overstated and Overinterpreted, and What to Do about It, *Bulletin of*
976 *the American Meteorological Society*, 97, 2263-2273, 10.1175/BAMS-D-15-00267.1, 2016.
977
978